CONTROL OF BALANCE OF PLANT COMPONENTS FOR SOLID OXIDE FUEL CELL SYSTEMS WITH SENSITIVITY TO CARBON FORMATION

by

Matthew J. Kupilik

A thesis submitted to the Faculty and the Board of Trustees of the Colorado School of Mines in partial fulfillment of the requirements for the degree of Doctor of Philosophy (Electrical Engineering).

Golden, Colorado

Date _____

Signed: _____
Matthew J. Kupilik

Signed: _____
Dr. Tyrone L. Vincent
Thesis Advisor

Golden, Colorado

Date _____

Signed: _____
Dr. Randy L. Haupt
Professor and Department Head
Department of Electrical Engineering and Computer Science

ABSTRACT

Solid oxide fuel cell systems have the potential to provide efficient, low greenhouse gas emitting power without the availability problems of both wind and solar energy. SOFC systems operate at high temperatures (> 600 C) in order to reduce ionic transport losses through a ceramic electrolyte. The benefits of the ceramic electrolyte include not requiring platinum based catalysts and a robustness to fuel composition. However such high temperatures create engineering challenges in construction, operation, and durability of the system as a whole. Both fuel and air must be pre-heated prior to entering the fuel cell stack. In order to ensure that carbon does not build up and degrade the system some form of fuel preprocessing is required. To move air and fuel through the system, blowers and valves must be used. Additionally during system start up, a method for pre-heating the fuel cell to within an operating range is required. All these components are tightly coupled to the time response and overall performance of the system. They also all have constraints and operating ranges, for example the fuel reformer must remain within a set temperature range or risk damage. Thus model predictive control is a natural choice to ensure that the maximum load following and overall system efficiency can be maintained without damaging components. This thesis analyzes system wide control of a solid oxide fuel cell system comprised of a tubular stack bundle, fuel reformer, air pre-heat exchanger, tailgas burner, and air blowers. Control oriented, dynamic component models have been created, allowing for estimation of temperatures and gas compositions throughout the system. The effects on system response of each component is analyzed, providing insight into realizeable response to load changes and sensitivity to noisy input parameters such as varying fuel stocks.

TABLE OF CONTENTS

LIST OF FIGURES

LIST OF TABLES

LIST OF SYMBOLS

Mass of the gas mix . . . . . m_{gas}

Density of the gas mix . . . . . ρ

Volume of the gas mix V

Mass flow of gas mix into reactor . . . . . $\dot{m_{in}}$

Mass flow of gas mix out of reactor . . . . . $\dot{m_{out}}$

Total system enthalpy . . . . . h_{sys}

Heat flux of the reactor . . . . . Q_{loss}

Bias in CH_4 . . . . . b

Coefficient of convective heat transfer . . . . . k

Surface area of control volume . . . . . A

Active site density of catalyst . . . . . γ

Reformer temperature . . . . . T

Inlet gas mixture temperature . . . . . T_{inlet}

Power to the reformer blower . . . . . P_{blo}

Power to the stack blower . . . . . P_{stack}

Mass of fuel sent to the reformer . . . . . m_{fuel}

Voltage of the stack V

Current delivered by the stack I

Temperature of the MEA . . . . . T_{MEA}

LIST OF ABBREVIATIONS

Balance of Plant	BOP
Carbon Deposition Barrier	CDB
Computational Fluid Dynamics	CFD
Catalytic Partial Oxidation	CPOX
Continually Stirred Tank Reactor	CSTR
Differential Algebraic Equation	DAE
Extended Kalman Filter	EKF
Heat Exchanger	HX
Linear Parameter Varying	LPV
Membrane Electrode Assembly	MEA
Multiple Input Multiple Output	MIMO
Model Predictive Control	MPC
Ordinary Differential Equations	ODE
Polymer Electrolyte Membrane	PEM
Proportional-Integral-Derivative	PID
Pseudo-Random Binary Signal	PRBS
Single Input Single Output	SISO
Solid Oxide Fuel Cell	SOFC
Variance Accounted for	VAF

ACKNOWLEDGMENTS

I would like to thank my wife, Agneta. Your contributions to my life are unbounded. Your patience and support throughout my time at the Colorado School of Mines has made this work not only possible, but pass almost too quickly. As long as you are present I look forward to whatever the future holds.

CHAPTER 1

INTRODUCTION

Solid oxide fuel cell (SOFC) systems have the potential to provide efficient, low greenhouse gas emitting power that is dispatchable without the variable availability of both wind and solar energy [1]. SOFC systems utilize a ceramic electrolyte, most commonly ytrria stabilized zirconia (YSZ). The YSZ electrolyte conducts oxygen ions, O^{2-} from the oxidizing environment of the cathode to the reducing environment of the anode. The global reactions that occur within the cell are:

$$\text{Anode:} \quad H_2 + O^{2-} \rightarrow H_2O + 2e^- \tag{1.1}$$

$$\text{Cathode:} \quad \tfrac{1}{2}O_2 + 2e^- \rightarrow O^{2-}. \tag{1.2}$$

In order for the solid ceramic electrolyte to sufficiently conduct oxygen ions, it needs to be at a high operating temperature. This high operating temperature (> 850 K) provides both benefits and challenges to operation. Low cost ceramic electrolytes can be used (without requiring platinum as a catalyst). The lack of a platinum catalyst results in a significant cost reduction over lower temperature polymer electrolyte membrane (PEM) fuel cell systems [2]. Additionally, the stack is able to handle a variety of fuels [2], overcoming another challenge faced by PEM fuel cell systems. SOFC systems can be fueled with biogas, methane, or other hydrocarbon fuels, allowing their use without the existence of a hydrogen fuel infrastructure [3].

However, such high temperatures create engineering challenges in construction, operation, and durability of the system as a whole. Both fuel and air must be pre-heated prior to entering the fuel cell stack, lowering efficiency and increasing system complexity. In order to ensure that carbon does not build up, deactivating reaction sites and reducing the ion conductivity of the electrolyte, some form of fuel pre-processing is required, increasing system

complexity [4]. This need for fuel pre-processing increases when the system is operating at low temperatures [5]. In order to move air and fuel through the system, blowers must be used, further decreasing efficiency. Additionally, during start up operation, the fuel cell must be pre-heated to within an operating range, which greatly lowers response speed and increases control complexity. Durability of the system is also impacted by temperature gradients and cycles throughout the lifetime of the system [6]. The engineering challenges presented by combining these systems in a durable package are what currently keeps SOFC systems from being cost effective when compared to traditional fossil fuel energy systems, or even wind and solar systems.

Feedback control of SOFC systems allows for the mitigation of some of these design challenges. Cell temperatures and gradients can be kept within limits proscribed by the materials available. Carbon deposition can be reduced by ensuring the inlet gas composition does not favor the formation of solid carbon at the current temperature. The impact of changing fuel stocks can also be adjusted for, ensuring the required power is met without exceeding reformer temperature constraints. All these limits can be met while exploring the trade off between system efficiency and load following ability.

1.1 Problem Statement

There currently is no published system level control algorithm that simultaneously maintains stack and reformer temperature, allows for load following without fuel starvation, prevents carbon deposition in the cell, and is robust to varying fuel composition. The primary goal of this research is to demonstrate the feasability of such a control system, while maximizing the applicability of such an algorithm to as wide a range of system configurations as possible. In order to meet the primary goal, three secondary objectives must be met. A suitable dynamic model of the complete SOFC system with balance of plant (BOP) components is required. The developed model then needs to be reduced to a control oriented model. Finally, the system control algorithm is implemented and its performance analyzed. These three objectives, development of the dynamic model, system reduction, and implementation

of the control algorithm are discussed below.

1.2 Dynamic Model of an SOFC System

All solid oxide fuel cell systems require fuel, air, and a way to regulate temperature. These fundamental requirements have resulted in several components being considered indispensable to the system. To ensure the research is applicable to many types and sizes of SOFC systems, we have focused on a study system consisting of just these minimum components. The components considered in this dissertation are: air blowers, fuel reformer, SOFC stack, tail gas burner, and a heat exchanger. The study system is shown below in Figure 1.1. A dynamic model for each component is created and all components are simulated together, ensuring all mass and energy balances are consistent throughout. The dynamic model is then reduced in order to create a tractable control problem. Utilizing the reduced model, a control system is developed providing for operation within system constraints as well as load following.

The energy conversion component is the SOFC stack; in the system under consideration, a tubular stack bundle is chosen. The tubular stack is a combination of a number of tubular cells. Planar geometries are also possible but require a longer start-up time in order to reach operating temperatures and are more susceptible to damage from thermal gradients. In order to produce a useable current and thus power a load, each cell within the tubular stack requires sufficient mass flow of fuel and air. Thus the stack consists of tubes connected in parallel with respect to mass flows. However, the voltage available from each individual cell is very low, approximately 0.6 to 0.7 volts, to overcome this limitation, each cell is connected in series with respect to voltage.

Also included in the study system is a fuel reformer which allows for the use of a variety of fuels, including biogas. Fuel reforming is the process by which a hydrocarbon fuel is converted into a hydrogen rich gas suitable for use within a fuel cell system. SOFC systems at high temperature allow for internal reforming, which involves feeding the hydrocarbon gas directly into the cell. Internal reforming avoids the use of a fuel reformer, but increases the

susceptibility of the cell to solid carbon formation and reduces the ability of the system to operate robustly to disturbances in the inlet fuel composition. The inclusion of a fuel reformer allows for greater control over the fuel composition that is fed into the cell and allows for operation without solid carbon formation for a wider range of temperatures. Thus, as SOFC temperatures continue to decrease in order to allow for much cheaper materials, the need for fuel reforming increases [5].

Methods of external reforming vary widely and have a large impact on load following and efficiency of the system. Three common methods of external fuel reforming include steam reforming, catalytic partial oxidation (CPOX) reforming, and auto-thermal (which combines steam and CPOX reforming). These methods of reforming are most often compared by looking at the yield of H_2 of the reformate over the total moles of all gas species present in the reformate. Utilizing this measure, steam reforming appears to be the most attractive as it has the highest H_2 efficiency (76% for dry CH_4) [2]. However, there are design considerations that would lead to the choice of other reforming methods. CPOX reforming has a much faster dynamic response and is an exothermic reaction, this makes it more appealing for load following applications and allows for pre-heating of fuel. CPOX reforming also does not require the addition of steam, which can be problematic for mobile systems. Auto-thermal combines the two reforming methods, utilizing the heat from the exothermic CPOX reaction to help simplify thermal management. It still has the disadvantages of requiring steam and having slower dynamics. The system in this work is simulated around a potentially mobile small scale system, of approximately 1.5 kilowatts. For the reasons above, the reformer method utilized is a CPOX reactor utilizing a foam supported rhodium catalyst.

A heat exchanger ensures that the inlet air is of sufficient temperature. High temperature SOFC systems require heat exchangers capable of operating upon gas flows with temperatures of up to 1200 K. Since thermal management is a major design challenge there is no standard geometry or design for such systems. Mobile SOFC systems also generally have heat exchangers that are tightly integrated and possibly combined with fuel reformers and

stack shell designs. Large increases in efficiency can be gained by ensuring all possible waste heat from reforming and other processes is used to preheat and maintain the high operating temperatures required. Modeling the heat transfer properties between all of these components from a first principles standpoint represents a considerable challenge, and is possibly impossible without completely specifying a system geometry. For these reasons most SOFC models greatly simplify the heat transfer properties of the system (the model in this work included). Dynamic models are still possible by assuming simplified geometries, such as simple tubular counter flow, whose physical parameters can by chosen to represent the actual heat transfer characteristics of an integrated system. Significant modeling and control work remains in the thermal integration of SOFC systems.

Mass flow throughout the system is primarily driven by two blowers. One blower to provide air to the stack and one to provide air to the fuel reformer. The air blowers are included as they influence the dynamic response and power output of the system. The rate at which air and fuel can be supplied are generally slower than the reaction dynamics in both the fuel reformer and stack. As such the ability to avoid unsafe operating conditions while increasing or decreasing the output current is very dependent on how quickly the amount of air and fuel can be changed. The fuel itself is considered to be at sufficient pressure and is not moved using a blower.

A tail gas combustor is included for system preheat and to make use of any unused fuel in the device. The complete use of all H_2 generally indicates that the whole surface area of the tube is not being employed and can result in damage. Since there is still additional fuel (H_2) present in the exhaust, in order to increase efficiency it can be combusted to raise the temperature of the exhaust gas, and thus the ability of the heat exchanger to pre-heat the incoming air.

Additional components that are often employed in SOFC systems include turbines for combined heat and power applications (CHP), vaporizers for liquid fuel use, and energy storage and conversion. These components, although important are not considered in this

dissertation. CHP applications show promise for very high operating efficiencies, but require much larger system sizes, their use is impractical for mobile systems [7]. Vaporizers greatly increase the variety of fuels useable within an SOFC system. However, their use can greatly decrease system response time and require additional heating, or the addition of steam. If it is expected that natural gas or biogas is available, vaporizers are also not necessary.

Energy storage is a necessary component in any load following application. As energy storage is expensive, it is desireable to minimize the amount required, which is very application specific. For transportation use, the SOFC system may be required to go from almost zero energy conversion to near full output in as short a time as possible. For such systems, a large amount of energy storage is required. For stationary implementations the load may vary much slower, as such less energy storage is required. The type of energy storage is also application specific. The use of ultracapacitors, batteries, hydrogen generation, pumped hydro, and a plethora of other methods are all possible and it is not clear what methods provide the most storage and response time for given applications. Hydrogen generation and pumped hydro are also infeasible for mobile systems. In order to model as general a system as possible, the energy storage is considered to be decoupled from the SOFC system considered. As such this thesis primarily analyzes the ability of the SOFC system to produce a current and respond to changes in the current demanded. The sizing of energy storage elements would then be based off the specific power needs of each application. As the fuel cell system generates DC power, if AC power is required, it is assumed sufficient inverter capacity is available. The power electronics to make this conversion are also not included in this dissertation. The dynamic model incorporates all of the above components and is of sufficient resolution that all the variables important for control can be estimated.

1.3 SOFC System Model Reduction

Although the non-linear system model can be considered low order compared to high-dimensional computational fluid dynamics (CFD) models, it is still quite complex, involving large systems of ordinary differential equations and differential algebraic equations. It is

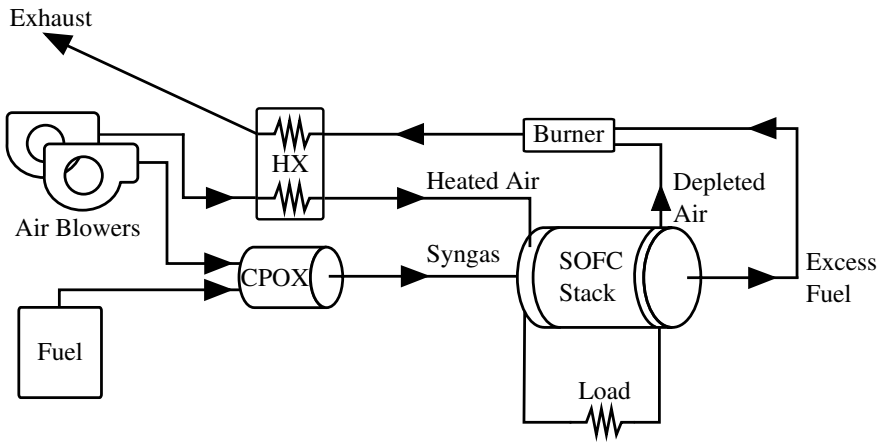

Figure 1.1: SOFC system block diagram.

thus not suitable for immediate use in a model based controller, where only the dynamics around the current trajectory are needed and many model evaluations at each time-step are required. Thus to meet the second objective, the non-linear system model must be reduced to a lower order model that still sufficiently captures the system dynamics. This reduction is accomplished via a technique used for system identification of linear parameter varying (LPV) models. An LPV model consists of a set of linear models that are combined using a function of a measurable parameter variable. The identification produces a single linear parameter varying model suitable for model predictive control (MPC).

System identification is a method to determine a model that matches the data produced by a physical system. The model structure utilized by the identification method can vary and need not be related to the actual physics of the system being studied at all. What is desired is a method to produce a model from only input and output data. Several considerations arise in the system identification process, specifically, what sort of experiments produce useable output data, and what form of model should be identified? Experiment design represents the choice of inputs and how they are excited. Possible input sequences could include step functions, pseudo-random binary sequences (PRBS), auto-regressive moving average processes, and periodic signals. Traditional identification methods often employ single input-output pair identification with the identification of linear time invariant (LTI)

models in mind. However, very accurate single input-output models can be found that show significantly worse performance when multiple inputs are excited simultaneously. Thus the choice of single input, single output (SISO) or multiple input multiple output (MIMO) experiments is important. What is desired of an input series is it be persistently exciting. That is, the generated output has sufficient information to capture the dynamics we want to model. Certainly the dynamic modes that need to be captured need to be excited. If the experiment is run only over several seconds, little information on a temperature dynamic that operates on the order of tens of minutes will be present. Time-steps need to be chosen such that system responses are excited and reach steady state. This can be challenging if the system exhibits a large range of time constants, as is the case for SOFC systems. The choice of experiment thus needs to focus on the control variables that will act as constraints or that need to be manipulated.

Also relevant is the idea of adequately exciting, which implies the output contains sufficient information to separate amongst models in the set of possible models being identified. This requires the choice of a class of model, or a structure imposed upon the identified model. There are again a wide variety of model choices available. Both linear and nonlinear models can be identified, with the desired control method being a deciding factor on which to identify. The number of inputs and outputs are often fixed, with the inputs selected as the variables that can be actuated and the outputs selected as the variables that can be measured. Additionally, if the identified model is being found from an existing higher order model, outputs can be selected that are not measurable in a physical system, thus allowing for their estimation and possible inclusion within constraint sets (these outputs still must be observable). Beyond the structure of the model, the model order is also a design consideration. The number of states required can be estimated using some identification methods, while for others it is a user set parameter. Increases in the state size also increase the model complexity, a consideration if the model is to be used within an on-line controller. Although mathematical frameworks are available for most of these issues, there are no hard and fast

rules. There is considerable flexibility and it is not always clear which model structure or sizes produces the most accurate identification results.

Linear parameter varying (LPV) models represent a specific model structure that can be chosen for an identification experiment. LPV approaches have grown out of the result that many systems can be approximated well with a linear time invariant (LTI) system at a specific operating point. LPV models allow for the extenstion of many results from LTI system theory to more complex problems involving constraints and non-linearity. They are also amenable to the use of state space representations, which is extremely useful if standard MPC software is to be used for control. The fundamental idea behind an LPV model is the identification of two or more linear models of a selected order and input/output size. These linear models are then combined using a function of a measured quantity. This measured quantity is henceforth referred to as the scheduling variable and varies in dimension depending on the number of linear models to be combined, and how they are to be combined. A common approach, and the one utilized in this work, is to assume an affine dependence of the state space matrices (A,B,C,D) on the scheduling variable. The state space matrices determine how the states (x) and outputs (y) change over time for given input (u)

$$\dot{x} = Ax + Bu \tag{1.3}$$
$$y = Cx + Du. \tag{1.4}$$
$$\tag{1.5}$$

In effect the scheduling variable is used to interpolate between a set of identified models. The result of the model structure is a state space linear model at every time-step that the scheduling variable is measured. This state space model changes affinely with respect to the scheduling variable and the identified LPV model.

1.4 Model Predictive Control

The third objective of the project is to implement a hierarchical control scheme using MPC (also known as receding horizon control) at the highest level. MPC approaches the

control problem from an optimization framework. This control strategy implements the actuator commands that are predicted by a model to minimize an objective function subject to constraints. The model determines how states evolve and how outputs are related to those states. For a linear model and quadratic cost function, the optimization problem takes the form:

$$\begin{aligned} J = \underset{u}{\text{minimize}} \quad & x'_{k,N} P_f x_{k,N} + \sum_{i=0}^{N-1} x_{k,i}^T Q x_{k,i} + u_{k,i}^T R u_{k,i} + \parallel Q_Y (y_{k,i} - y_{ref,i}) \parallel_2 \\ \text{subject to} \quad & y_{k,i} \in Y \; i = 0, \ldots, N-1 \\ & u_{k,i} \in U \; i = 0, \ldots, N-1 \\ & x_{k,i+1} = A_k x_{k,i} + B_k u_{k,i} \\ & y_{k,i} = C x_{k,i} + D u_{k,i} \\ & x_{k,i} \in \chi \; i = 0, \ldots, N-1 \end{aligned} \tag{1.6}$$

The optimization problem given in 1.6 is then to determine a minimal sequence of inputs that drives the outputs to the desired values while not violating constraints. In Eq. 1.6, $x_{k,i}$ is the system state at time-step k, and horizon step $i = 1...N$ and is constrained to exist in the set χ. The state and output also evolve according to the system dynamics defined by the state space matrices A,B,C, and D. The system outputs at time-step k and horizon step i are $y_{k,i}$ and are constrained to Y. The outputs at time-step k and horizon step i are $u_{k,i}$ and are constrained to U. Matrices Q, R, Q_y are weighting matrices that give preference to certain states, inputs, or specific outputs. The P_f matrix is a final state weighting that enforces stability.

There are many variants to the cost function in 1.6, including non-quadratic cost functions, depending on the norm used. The advantage to using a quadratic cost function is the availability of a large number of highly efficient and well developed solution methods with public implementations. Convexity can also be guarenteed with selection of positive semi-definite weighting matrices. The specific cost function utilized is highly dependent on the goals of the control algorithm and the system being controlled. MPC has many advantages in that it easily handles constraints, which are not handled in LQR (linear quadratic

regulator) or most proportional-integral-derivative (PID) methods. It is also not complex to implement the control law, the optimization problem simply calculates the values of the inputs to be applied at the next time-step. Disadvantages of MPC include a possible increase in processing time, and a lack of theoretical results on feasability and stability for the use of LPV models. This same lack of theoretical results also makes performance guarantees difficult. Perhaps the single largest disadvantage for MPC, however, is the requirement of a model accurate enough for control, and fast enough to be optimized in real time. First principles models are difficult and time consuming to create, and are rarely fast enough to be used within a control loop.

MPC techniques were developed in order to control constrained multiple input multiple output (MIMO) systems in the oil and chemical industries, so it is a natural application to the chemically reacting flows in reforming and the electrochemical reactions in fuel cells. The fast electrochemical and chemical responses present in the reformer and stack are combined with the much slower fuel/air delivery and temperature systems. The ability of linear MPC to control the system is thus directly related to the existence of an accurate linear model representation of the system. Given such a model, the MPC controller will determine the set points for the air blowers and the fuel mass flow based off the estimation of the fuel composition into the stack, the predicted stack performance, and the heat exchanger and tail gas burner estimate of the new input air temperature.

1.5 Contributions

The research provides a linear parameter varying plant model suitable for meeting constraints not just in the stack but on the components themselves. With a control strategy in place, several important questions about the performance of solid oxide fuel cells are answered:

- What effect do the BOP components have on the time response of the system to load changes?

- What components act as bottlenecks to system response?
- What load changes can be met while still ensuring all operating limitations are maintained?
- Is the system robust to disturbances in inputs? For example, if the inlet fuel composition varies over time, can the system compensate?
- What numerical and implementation issues are present in applying this LPV identification approach?

In addition to answering these questions a contribution of this thesis is the demonstration of a control algorithm unique in the following aspects: utilizes MPC on a reduced LPV system wide model and incorporates fuel composition constraints on the CPOX reformate.

CHAPTER 2
PRIOR WORK

This chapter will review prior work within the three goals of this dissertation. Initially, the current state of first principles control oriented SOFC system models will be examined. The development of system identification within an LPV framework is presented. Finally, existing research on the use of MPC and other control methods for SOFC systems is covered.

2.1 SOFC Modeling for Control

Modeling SOFC systems requires both the development of accurate stack/cell models as well as the integration of the stack into systems with balance of plant components that are connected by mass flows and thermal interaction. For SOFC systems thermal integration modeling has proven to be essential for achieving high efficiencies as well as durable, stable systems. Initial modeling of cells and stacks has led to the development of a multitude of lumped, thermodynamic models of SOFC stacks [8–11]. Although useful for predicting dynamic outputs for given fuel flow and stack temperature, such models have to make large assumptions of temperature uniformity across the stack. Since system failure due to thermal cycling and large temperature gradients within the stack is currently a design challenge, temperature uniformity is a poor assumption. More recently higher order dynamic models taking into account variable compositions and temperatures within the stack have become more developed and available for control use [12–14]. These one dimensional models incorporate species conservation and thermal effects along a discretized tube or plane. The response of these models are highly dependent on the geometry of the cell as well as what reaction mechanisms are included. Utilizing a spacial model requires assumptions on the size and geometry of the system, which reduces the generality of the model.

This thesis is focused on the effects of balance of plant components and system control on stack performance. Stack geometry and size does impact the magnitude of air and fuel

flows that are required and thus the size of the blowers, fuel processor and heat exchanger along with their dynamic response. The greater accuracy achieved by utilizing spatial models incorporating chemical kinetics is required to enable the controller to avoid violating operating constraints. So this loss of generality is required in order to suitably control the system. However, since the control algorithm is constructed from a system identification of the high order models, it is possible to extend the approach for any stack model size and geometry by repeating the identification experiments and producing a different LPV model.

Due to dependence on temperature and composition of inlet gasses, load following or other performance optimizations are highly coupled to the additional components in the system and the thermal exchanges between them. Either a system level model is required, or non-realistic assumptions have to be made in order to implement viable control strategies. The focus on system level control models for SOFC systems is still the subject of a large amount of research. For example, Mueller et al. [15] developed one dimensional flow models of a fuel reformer, tubular cell, and integrated heat exchanger. The system model is verified against a physical system and provides several insights into the dynamics of a SOFC system when coupled with a steam reformer, combustion chamber, and dissipator. Primarily, the impact of fuel flow delays on changes in current demand are indicated as a limiting factor in load following. Murshed et al. [16] describes a one dimensional flow model of a planar stack and combines it with lumped models of a steam fuel reformer and heat exchanger. The objective of the system modeling is for control purposes and assumptions are made on flow temperatures to ensure only ordinary differential equations (ODE) are employed. Such assumptions avoid the requirement for further system reduction, but reduce the model accuracy. Stiller et al. [17], combined lumped models of a fuel reformer and gas turbine with a dynamic model of a counter flow heat exchanger. This work also analyzed the impact of expected cell degradation on stability. Simulated load changes were met very quickly; a load change of 53% of the operating range was met within approximately 100 seconds. No kinetics are used in the reformer and the system is required to operate at a fixed steam to carbon

ratio. In Mueller et al. [18] transient dynamics of the system as a whole are considered and a feedback control algorithm is shown to provide load following on a simulated system. A non-dimensional analysis is done to determine what transient limits are present on the fast electrochemistry by flow delays caused by components such as blowers and fuel reformers. Their conclusion is that delays in fuel caused by reformer dynamics are the primary limitation of SOFC load following ability. It should be noted that all these works simulate different system sizes and configurations. Further, only Mueller et al. [15] presents verification results for a physical system. As such, the different modeling approaches are difficult to compare.

2.2 System Identification for LPV Systems

An LPV system is one which the dynamics (A, B, C, D matrices for a state space model) are determined by a function of a known scheduling variable. System identification of LPV systems can generally by classified under two methodologies: global and local. Local approaches identify standard linear models at operating points, generally by inducing random perturbations around that point. This identification procedure is repeated until a set of models is available, one for each operating point of the system. Once a set of linear models are available, each at a different operating point, a measured variable is used to interpolate between them. The interpolation is usually weighted to avoid rapid changes in system dynamics. These approaches developed out of gain scheduling techniques [19]. Examples of this system identification method have been applied to a wide variety of processes. In Groot Wassink et al. [20] polynomial interpolation was applied to create a LPV model for a wafer manufacturing process. The work of Zhu and Xu [21] also developed a polynomial interpolation for more general non-linear systems. Interpolation techniques have also been applied to SOFC stack models, where the current is used to interpolate between state space models, such as in Sanandaji et al. [22] (using the same stack model as this dissertation).

Whatever quantity is chosen as a scheduling variable, it must contain enough information to distinguish the current system dynamics so that the LPV model can be blended from amongst the different linear models in the identification set. For some systems physical

insight can be used to choose a scheduling variable, if a measured physical parameter clearly differentiates between different sets of system dynamics. For example, Yung [23] used stiffness and flexibility analysis (calculated from measured joint accelerations and positions to schedule a linear model applied to a robotic platform. Flow control for dam outlets also forms a nonlinear problem where the spatial characteristics can be used to interpolate between a set of linear models, as was done in Puig and Quevedo [24] using the upstream flow as a scheduling measurement. The use of physical insight into the scheduling is effective when available, however, it requires a strong understanding of the model and physical principles involved. Often there is no clear physical variable or calculated parameter that provides a clear delineation between operating modes of the system.

True for all local interpolation methods is that the dynamics of the system between the locally identified operating points are only approximated. Additional operating points can be used, but at the cost of increasing complexity. Global subspace methods try and account for this by fitting linear models to data sets generated over the entire operating range. Such methods use a reconstruction of the state and an extended observability matrix to recreate the system matrices. Subspace methods are well developed for the LTI case ([25]) and recent work has extended these methods to LPV models. The linear spaces upon which these algorithms must operate unfortunately explode in dimensions quickly with increasing problem size. Approximations in the state sequence can be made which introduce a bias, as in Verdult [26]. Methods to avoid this bias were developed also in Verhaegen and Yu [27] requiring the scheduling sequence to be periodic. This is a strong restriction, and eliminates large classes of non-linear systems. A kernel method was also introduced in Verdult and Verhaegen [28] to reduce the dimensionality requirement such that useable sizes of models could still be identified. An implementation of this method (which is also employed by this dissertation) can be found in Wingerden [29].

2.3 Control for SOFC Systems

In implementing a control strategy for a SOFC system, feedback based algorithms can be implemented on each component or combination of components, or some form of model based control can be used. Component level feedback control most often consists of PID loops. A PID approach initially calculates the difference between the output and a reference or desired value. The actuator command is then changed proportionally to this difference, or error. The derivative term is added to reduce the actuator command proportional to the derivative of the output. If the output is changing very fast in the right direction the controller will reduce the actuator command, if the output is changing very slowly, the actuator command will be proportionally increased. The integral component changes the actuator command proportional to the accumulated error. This control action helps eliminate steady state error, although it can also increase overshoot. Although PID is the most widely implemented mode of process control in industry today, it has several drawbacks when applied to SOFC systems. Amongst these is linearity of the control action, which causes problems in applications with nonlinear dynamics. Also a concern is the lack of constraint handling, which is a requirement for SOFC control. These difficulties can be overcome, but require multiple loops and ad-hoc system specific implementations to achieve reasonable performance. Studies of system level feedback control include Sorrentino and Pianese [30], which focused on start up conditions, and utilized PID loops to actuate valves controlling mass flows. Another feedback approach was used in Stiller et al. [17] for implementing load following with separate loops to regulate temperature. Although PID control has been shown to function at local operating points, in order for a controller to be valid over the entire range of operation as well as exhibit robustness to input noise, some form of non-linear control is required.

If model based control is chosen, several approaches are available. If a physical system is available, system identification can be performed and a control model over the desired operating range can be produced. No examples of this technique were found in the literature. Alternatively, a first principles physics based dynamic model of each component can be

created and combined for a dynamic model of an entire fuel cell system. Once a high order first principles model is available, either a system identification can be carried out or a neural network model created. This is done in order to produce a low order model of sufficient speed to be used within the controller. Both of these approaches are represented in the literature. The control oriented model can also then be combined with feedback methods or used within some form of optimal control (such as MPC). Model based feedback methods are well represented in the literature. In Aguiar et al. [31] a feed-forward controller (based on a model) is used to vary fuel and air flows while a PID loop is used to regulate temperature by changing the air flow rate. Mueller et al. [15] uses a model "look up" approach to regulate the air and fuel flows to regulate current. This study also performed an experimental validation using a Westinghouse SOFC system. Pukrushpan et al. [32] performed a system wide analysis of feedback control for PEM based fuel cell systems which have much different temperature regulation requirements. Feedback can also be used with a model to address constraints. In Fardadi et al. [33] a H_∞ feedback approach is used to minimize thermal gradients in a planar cell. A feed forward approach to achieve the same temperature gradient minimization was carried out in Inui et al. [34]. Although neither approach guarantees the temperature variation will be within limits, it does optimize the inputs to reduce the temperature gradient. Neural networks offer an alternative to the system identification approach proposed here. In Wu et al. [35] an artificial neural network was created and used to control fuel utilization, showing an improvement over operation with fixed fuel usage. Artificial neural networks provide an alternative structure to mathematical models, instead utilizing a statistical data based method of predicting outputs. As such they are prone to overfitting and also require multiple datasets for training weights and validating the network.

Optimal control is also being researched in response to existence of constraints on both inputs and outputs. Bhattacharyya and Rengaswamy [36] utilized a system identification approach based on a validated model combined with MPC, however, this approach was limited to the stack. Sanandaji et al. [37] also performed a system identification on a high

order stack model combined with MPC. This study also took into account the wide range of operating points and combined multiple linear models into a single LPV model with good load following and thermal management. Again, however, only the stack was modeled, with BOP components considered only as first order delays. System level MPC remains an open area of research. In Murshed et al. [38] linear MPC is applied to a system model linearized around an operating point, additionally, non-linear MPC is used after discretizing the model (which in this case is a set of first order ODEs). Non-linear MPC requires additional computing resources, especially for a real time implementation. Although Murshed et al. [38] has shown non-linear MPC to be superior to linear MPC at a set point, no comparison is made to linear MPC using a LPV model implementation. The use of a LPV model and the inclusion of reformer constraints and blower inertia are important differences between this research and that presented in Murshed et al. [38]. System level SOFC control using MPC was applied in Spivey and Edgar [39] to multiple input, single output (MISO) identified transfer functions calculated for each control variable.

2.4 Contributions in Relation to Existing Work

In comparison to the existing literature, unique aspects of this thesis include controller robustness to an unknown inlet fuel composition, the inclusion of composition based constraints within the system controller, and the use of an LPV model reduction applied to the system as a whole. Robustness to unknown fuel composition is important in the case of a biogas fed stack and is accomplished with an extended Kalman filter. Gas compositions are calculated from the inclusion of surface chemistry in the fuel reformer, and a high order model of the fuel cell stack. These fuel compositions allow for reformate constraints to be included within the controller. Constraints include ensuring the reformate does not form solid carbon at the current operating temperature. In order to include constraints within the controller, a LPV model reduction is performed which allows for the use of linear MPC while still being valid over all desired operating conditions.

CHAPTER 3

SYSTEM LEVEL MODEL

Since the main effort of the research is to determine the effect of BOP components on control of the SOFC system, sufficiently detailed dynamic models are needed for all components. Once a model is in place that allows the simulation of all the variables of interest, including their constraints, a model reduction process can be carried out. The model reduction creates a set of linear models that are blended into one LPV model whose system matrices are calculated based on a scheduling variable. Using only a stack model Sanandaji et al. [37] showed that output current alone provides an accurate method of scheduling. However, additional measurements are available and can also be incorporated into the scheduling variable. This work tested a combination of scheduling variables, including the current, the temperature of the MEA assembly, and the temperature of the fuel reformate. The LPV model is then combined with linear MPC efficient enough for real time control. The individual component models are all sized appropriately for the overall system power ouput (approximately 1.5 kw).

The first challenge in developing a model to be used for model based control is determining the level of fidelity. Extremely high order CFD models can be created to match very specific geometries. CFD models capture both the spatial and time varying aspects of the system, such as Kattke et al. [40]. Such models are tailored very specifically to the geometries involved and impose a prohibitive computational burden. As such they are most suited as analysis and design tools rather than for control. At the opposite end of the fidelity spectrum, SOFC systems can also be modeled using only lumped thermodynamic models, enforcing mass and energy conservation, but ignoring spatial dynamics and chemical kinetics. Such models ignore the kinetics at the reformer catalyst and the cells. These effects are important to the operation of the SOFC system and cannot be ignored. Hot spots can occur spatially along

cell tubes [40], and the reformate composition is highly dependent on the reaction kinetics at the catalyst [41]. Both these factors impose operating constraints on the system. As such, the constructed system model needs to capture the variables which impose system constraints over the range of desired operating conditions. For a SOFC system this means that chemical kinetics within the reformer and stack are important. Thus, spatial models are used for the heat exchanger and SOFC stack while a lumped model of the CPOX is expanded to include surface chemistry. Inclusion of surface chemistry is an important difference between our reformer model and previous works [10, 16, 42], as much of the temperature response is due to the surface reactions as compared to the gas phase chemistry [43]. The blower model is lumped, but includes the important transient responses for the system. In the case of the blower, variables that influence the dynamic response are the motor inertia and the change in mass flow with respect to a change in motor power. The burner is modeled as a burner stabilized axisymmetric flame, which allows for simulation of the outlet composition and temperature to a varying inlet mass flow, composition, and temperature. In the next section the models for the system components illustrated in Figure 1.1 are described, starting with the SOFC stack.

3.1 SOFC Stack

This research makes use of a previously developed anode-supported tubular cell model developed by Colclasure et al. [13]. The stack model uses physical conservation equations to predict the coupled effects of fuel channel flow, porous-media transport, heat transfer, thermal chemistry, and electrochemistry on cell performance. The model outputs include spatial and temporal profiles of chemical composition, temperature, velocity, and current density. A mathematical description of the model can be found in Colclasure et al. [13]. The model is implemented in C++ and makes use of Sundials, a DAE equation solver [44]. Sundials utilizes a varying timestep in order to calculate the output variables from the initial conditions and inputs. The length of the simulation is set to the timestep for the SOFC model as a whole. The control volume considered is an axial slice, with each slice being $\frac{1}{100}$

of the total cell length. Initial conditions include the compositions, flows, temperatures and reaction variables for each axial discretization. Inputs include the mass flows, compositions, and temperatures for both the anode and cathode sides. As the model considers only a single cell, thermal effects from cell to cell are not included, only heat transfer to a fixed exterior temperature, with the exterior modeled as a CSTR. To model a stack, 100 tubular cells are connected electrically in series and in parallel with respect to mass flows. The sizes of the tubes are taken as 15 cm long with an outer diameter of 1 cm. SOFC stack parameters are summarized in Table 3.2.

3.2 Fuel Reformer

The fuel reformer consists of a CPOX reactor placed upstream of the stack. The purpose of the reactor is to take a hydrocarbon gas and reform it into a hydrogen rich reformate gas, or syngas. The model used is a zero dimensional CSTR modified to include surface chemistry. The geometry modeled is a rhodium coated tubular foam embedded inside a glass tube. The control volume used is the catalyst loaded foam and the material tube supporting it. An energy and mass balance is then used to predict the change in temperature over time based on the composition of the gas in the reactor, the oven temperature, and the current temperature of the catalyst. Assumptions include a uniform catalyst temperature, and that the surface coverages on the catalyst are at steady state for each timestep. The latter assumption is valid since the temperature dynamics of the reactor are much slower than the kinetics of the catalyst. Timesteps are chosen to capture the thermal dynamics, which are on the order of seconds, compared to fractions of a second for the catalyst kinetics [45]. The fuel input to the CPOX can be any combination of oxygen, nitrogen, methane, CO_2, hydrogen, or carbon monoxide. The mass and energy balance for the reactor from first principles, derived from mass of gas in the reactor is:

$$\frac{d(m_{gas,cx})}{dt} = \frac{d(\rho_{gas,cx} V_{cx})}{dt} = \dot{m}_{in,cx} - \dot{m}_{out,cx} \tag{3.1}$$

$$\frac{dh_{cx}}{dt} = \dot{m}_{in,cx}h_{in,cx} - \dot{m}_{out,cx}h_{out,cx} - Q_{loss,cx}, \tag{3.2}$$

where $m_{gas,cx}$ is the mass of the gas inside the reactor, $\dot{m}_{in,cx}$ and $\dot{m}_{out,cx}$ are the mass flows of gas into and out of the reactor. The density of the gas ($\rho_{gas,cx}$) and the volume of the reactor (V_{cx}) are assumed to be constant, so (3.1) gives $\dot{m}_{in,cx} = \dot{m}_{out,cx}$. The total system enthalpy is h_{cx}. The inlet and outlet enthalpies ($h_{in,cx}$ and $h_{out,cx}$) of the gas mixture are calculated using Cantera [46] and the reaction mechanism from Deutschmann et al. [41] and are functions (f_1 and f_2) of the mixture composition and temperature:

$$h_{in,cx} = f_1(n_{mix,cx}, T_{inlet,cx}) \tag{3.3}$$
$$h_{out,cx} = f_2(n_{mix,cx}, T_{cx}). \tag{3.4}$$

The heat loss is defined as:

$$Q_{loss,cx} = k_{cx}A_{s,cx}(T_{cx} - T_{env}) + \epsilon_{cx}\sigma A_{s,cx}(T_{cx}^4 - T_{env}^4), \tag{3.5}$$

where k_{cx} is the coefficient of convective heat transfer, $A_{s,cx}$ is the surface area of the reactor, and σ_{cx} is the coefficient of radiative heat transfer. σ is the Stefan-Boltzmann constant. Assumptions made in the heat loss equation include uniform heat loss across the control volumes boundary, uniform temperature inside the control volume (T_{cx}), and a uniform environment temperature outside the volume (T_{env}). The total system enthalpy h_{cx} is given by:

$$h_{cx} = m_{gas,cx}h_{gas,cx} + m_{solid,cx}h_{solid,cx} \tag{3.6}$$

where the gas subscripts indicate the enthalpy or mass of the the gas in the control volume. The total mass of the gas-phase mixture within the reactor is $m_{gas,cx} = \rho V$ and $h_{gas,cx}$ is the specific enthalpy (J/kg) of the gas-phase mixture. The mass of the solid phase is $m_{solid,cx}$ and $h_{solid,cx} = c_{p,s}T_{cx}$ is the solid-phase enthalpy, were $c_{p,s}$ is the heat capacity. These energy and mass balances are then used to predict the change in temperature over time, given the inlet composition to the reactor, the external temperature, and the current temperature of

the catalyst. The mass of the solid is known experimentally and detailed in Table 3.1.

3.2.1 CPOX Experimental Verification

This model is validated using an experimental CPOX reactor ([47]). The experimental system uses simulated biogas and air (no sulfur compounds). A schematic of the experimental reactor is shown in Figure 3.1. The catalyst used is rhodium supported on a ceramic foam. The inlet gasses are controlled via mass flow controllers (MFC) and mixed prior to entering the oven and catalyst. The reactor itself is contained within a separate temperature controlled oven. Type K thermocouples are placed just prior to the catalyst foam inlet and just outside the catalyst loaded foam outlet. An oven is used to set the environmental temperature of the reactor. The oven temperature is also measured and controlled via a type K thermocouple placed inside the oven near the reactor tube. The entire oven is sealed with thermal foam in order to minimize heat transfer to the lab. Measurements of the gas

Table 3.1: Reformer Experiment Parameters

k_{cx}	$18.236\frac{W}{m^2K}$
ϵ_{cx}	$0.333\frac{W}{m^2K}$
γ	$3.25 \times 10^{-6}\frac{mol}{cm^2}$
$m_{solid,cx}$	$.0057\ kg$
$Q_{k,cx}$	$\begin{bmatrix} 10 & 0 \\ 0 & .01 \end{bmatrix}$
R_{cx}	1

composition are made using a gas chromatograph (GC) downstream of the reactor. Any water present in the reformate is removed prior to the GC via a water trap. In order to determine the heat constants for the model (k_{cx},ϵ_{cx}), the externally controlled oven was used to vary the temperature of the reactor environment with no gas present. Since there was no reaction, the temperature response of the reactor allows the calculation of the heat transfer coefficients of the lumped model via a least squares fit. This method gives excellent agreement between our model and the measured thermal response of the reactor. Using the fitted

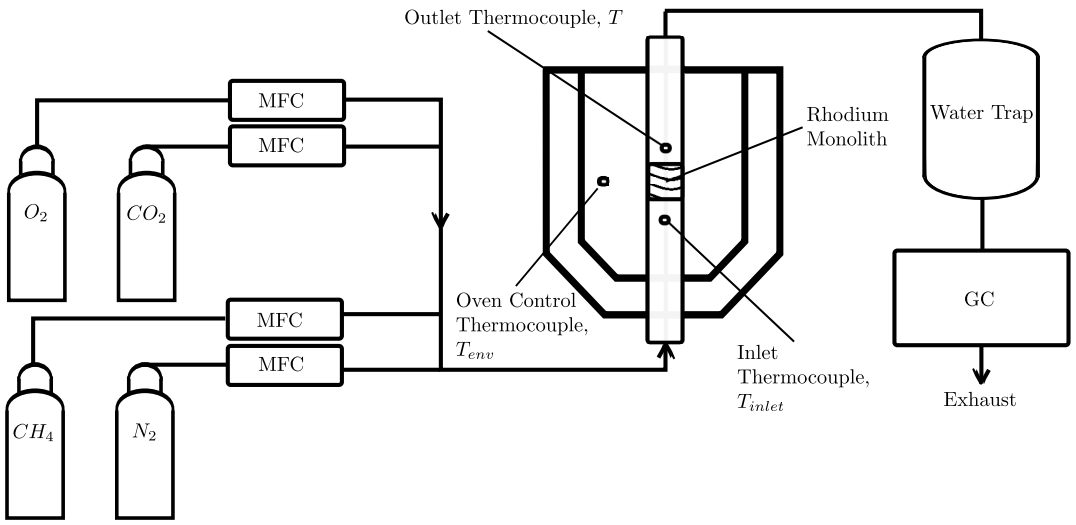

Figure 3.1: CPOX Experimental Setup

thermal constants, the catalyst parameters were then matched to the experiment. Constants used as tuning parameters were the active site density of the supported catalyst (γ). Tuning this parameter allowed for a thermal and reformate composition match between the model and the experiment. The calculated values for the heat transfer coefficient and the catalyst site density are shown in Table 3.1. The results of a start up condition, followed by an inlet step in $\frac{O_2}{CH_4}$ from 1.03 to 1.25, followed by system cool-down are shown in Figure 3.2. The thermal response of the model shows good agreement with the measured experimental response. Compositions are more difficult to measure, as real time measurements of gas compositions were not available with the gas chromatograph on hand. Steady state gas concentrations were found to match within 2%, after taking into account the removal of any water in the reformate output.

3.2.2 Inlet Fuel Estimation

In order to ensure the system is robust to unknown fuel variations the molar percentages of methane and CO_2 in the inlet stream are estimated using an extended Kalman filter. The estimated parameter is modeled as a bias, or variation from an assumed molar percentage of methane. Thus the ratio of CO_2 and CH_4 is allowed to vary by an unknown amount.

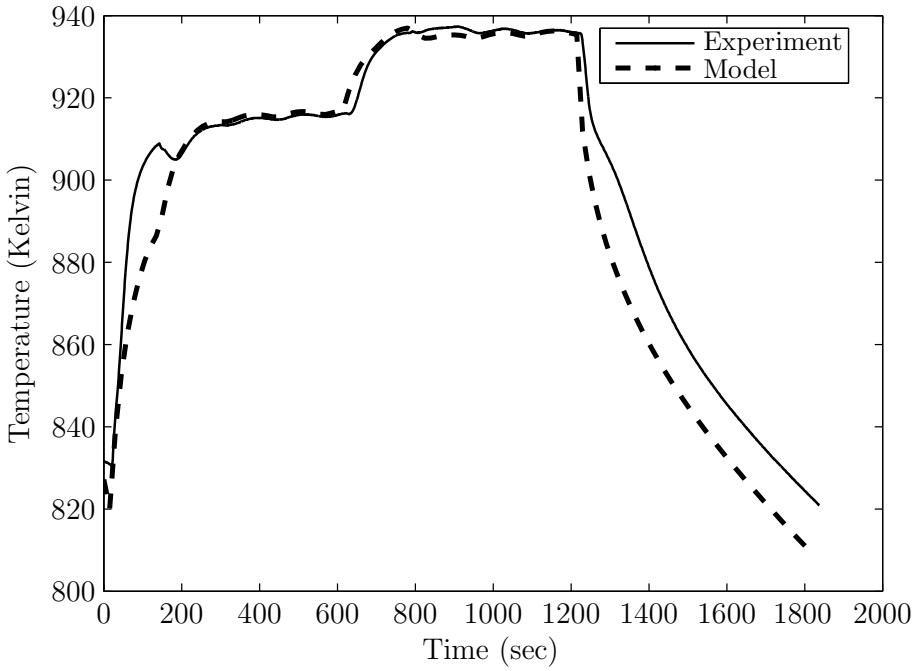

Figure 3.2: CPOX Reactor Temperature, Model Verification Results

This uncertainty is included to accurately capture the output of actual biogas production facilities, which can show large variations in the composition of biogas [48, 49]. A change in the inlet fuel composition, even for a fixed mass flow, can have a large impact on the CPOX temperature and composition of the reformate, and thus also on the current produced by the stack. The bias model quantifies the unknown gas composition in the inlet stream. We define μ as a reference percentage of CH_4 in the inlet fuel. This value is provided as an input to the control algorithm. The unknown bias (b) is then the change in CH_4 percentage from nominal, or μ. The system is a function of algebraic and differential constraints involving the system enthalpy h_{cx}, the reactor temperature, T_{cx} and the gas composition bias b. Define

$$x_{cx} = \begin{bmatrix} h_{cx} \\ b \end{bmatrix}, \quad u_{cx} = \begin{bmatrix} \dot{m}_{in,cx} \\ \mu \\ T_{env} \end{bmatrix}, \quad z_{cx} = T_{cx}. \tag{3.7}$$

Then (3.1), and (3.2) and (3.6) can be combined with additive process noise (v_{cx}), and measurement noise (r_{cx}), which are assumed to be zero mean, i.i.d. random sequences with covariances $Q_{k,cx}$ and R_{cx} respectively:

$$\begin{aligned} \dot{x}_{cx} &= f(x_{cx}, u_{cx}, z_{cx}) + v_{cx} \\ 0 &= g(x_{cx}, u_{cx}, z_{cx}) \\ y_{cx} &= z_{cx} + r_{cx}, \end{aligned} \tag{3.8}$$

where the functions f and g are defined to be:

$$\begin{aligned} f(x, u, z) &= \begin{bmatrix} \dot{m}_{in,cx} f_1 - \dot{m}_{out,cx} f_2 - Q_{loss,cx} \\ 0 \end{bmatrix} \\ g(x, u, z) &= h_{cx} - m_{gas,cx} h_{gas,cx} + m_{solid,cx} h_{solid,cx}. \end{aligned} \tag{3.9}$$

The system is a DAE with two differential states (the system enthalpy and the bias) and one algebraic state (reactor temperature). The system is also non-regular, since the constraints are functions of the control variables. Thus, depending on what is chosen for $u(t)$ the solution lies on a different manifold. That is, the constrained space that the state trajectories lie on depends on the inputs. Assuming we know h_{cx} as an initial condition, then the temperature at the next time step is the temperature at which the enthalpies and $Q_{loss,cx}$ balance. These are both functions of the temperature and the enthalpy is also a function of the gas composition. We can then use a Cantera CSTR reactor model and solve for the surface coverages and enthalpies of the outlet gas at a given temperature [46]. The bias is included in the state for purposes of estimation, allowing the use of an extended Kalman filter (EKF) to estimate the unknown inlet fuel composition with the modifications for first order DAE systems presented in Kumar Mandela et al. [50].

3.3 Heat Exchanger

Dynamic models capable of capturing the time response for high temperature micro heat exchangers are not commonly available. The design of such heat exchangers is also an ongoing topic of research for use in micro turbines. The high temperature of SOFC systems require the inclusion of nickel or other more exotic alloys [51], greatly increasing the cost. Heat exchangers for use in high temperaure fuel cells must also take into consideration large thermal stresses induced during start up and shut down procedures. The model implemented for this research is a simple dynamic counter flow heat exchanger model developed by Ansari

and Mortazavi [52], which can be adapted to the geometry of a much more complex multipass system with several assumptions. The design is assumed tubular and the model allows for variable inlet temperatures and mass rates of both flows. Using a first principles approach, combined with a discretization of the tube, the dynamic response of both fluids and the heat exchanger wall can be calculated. Assumptions in the model include negligible axial heat transfer in the wall via conduction and no heat transfer from the outer tube wall to the environment. The outer tube is referenced as subscript 1 and the inner tube is referenced as subscript 2. The energy balance for a single segment of the discretized heat exchanger length is:

$$\begin{aligned} C_{1,hx}\rho_{1,hx}A_{1,hx}\frac{\partial T_{1,hx}}{\partial t} &= -k_{1,hx}U_{1,hx}(T_{1,hx}-T_{w,hx}) - C_{1,hx}\dot{m}_{1,hx}\frac{\partial T_{1,hx}}{\partial x} \\ C_{w,hx}\rho_{w,hx}A_{w,hx}\frac{\partial T_{w,hx}}{\partial t} &= -k_{1,hx}U_{1,hx}(T_{1,hx}-T_{w,hx}) - k_{2,hx}U_{2,hx}(T_{w,hx}-T_{2,hx}) \\ C_{2,hx}\rho_{2,hx}A_{2,hx}\frac{\partial T_{2,hx}}{\partial t} &= k_{2,hx}U_{2,hx}(T_{w,hx}-T_{2,hx}) - C_{2,hx}\dot{m}_{2,hx}\frac{\partial T_{2,hx}}{\partial x}, \end{aligned} \tag{3.10}$$

where $C_{1,hx}$, $C_{w,hx}$, and $C_{2,hx}$ are the heat capacities of the outer fluid, wall, and inner fluids respectively. $A_{1,hx}$, $A_{w,hx}$, and $A_{2,hx}$ are the cross sectional areas of the outer tube, wall, and inner tube. $U_{1,hx}$ $U_{2,hx}$, and $\dot{m}_{1,hx}$, $\dot{m}_{2,hx}$ are the perimeters and mass flows of the outer and inner tube. $\rho_{1,hx}$, $\rho_{w,hx}$, and $\rho_{2,hx}$ are the densities of the outer fluid, wall, and inner fluid. The temperatures of each fluid are $T_{1,hx}$, and $T_{2,hx}$. Define the following dimensionless coefficients:

$$\begin{aligned} L_{1,hx} &= \frac{C_{1,hx}\dot{m}_{1,hx}}{k_{1,hx}U_{1,hx}} & D_{1,hx} &= \frac{\rho_{1,hx}C_{1,hx}A_{1,hx}}{k_{1,hx}U_{1,hx}} \\ L_{2,hx} &= \frac{C_{2,hx}\dot{m}_{2,hx}}{k_{2,hx}U_{2,hx}} & D_{2,hx} &= \frac{\rho_{2,hx}C_{2,hx}A_{2,hx}}{k_{2,hx}U_{2,hx}} \\ D_{w,hx} &= \frac{\rho_{w,hx}C_{w,hx}A_{w,hx}}{k_{1,hx}U_{1,hx}+k_{2,hx}U_{2,hx}}. \end{aligned} \tag{3.11}$$

The wall temperature is assumed to be constant within each segment, and is estimated from:

$$T_{w,hx} = T_{w,hx}(0) + D_{w,hx}\theta(1-e^{-t/D_{w,hx}}), \tag{3.12}$$

where θ is the time dependent temperature coefficient. This coefficient is found from the energy constraint on the wall. Substituting equation 3.12 into equation 3.10 and using the coefficients defined above gives two non-homogenous differential equations:

$$
\begin{aligned}
D_{1,hx}\frac{\partial T_{1,hx}}{\partial t} + L_{1,hx}\frac{\partial T_{1,hx}}{\partial x} + T_{1,hx} &= T_{w,hx}(0) + D_{w,hx}\theta(1 - e^{\frac{-t}{D_{w,hx}}}) \\
D_{2,hx}\frac{\partial T_{2,hx}}{\partial t} + L_{2,hx}\frac{\partial T_{2,hx}}{\partial x} + T_{2,hx} &= T_{w,hx}(0) + D_{w,hx}\theta(1 - e^{\frac{-t}{D_{w,hx}}}).
\end{aligned} \tag{3.13}
$$

These equations are linear with only a single unknown each and are solved via the Laplace transform as described in Ansari and Mortazavi [52] and Roetzel and Xuan [53]. Starting at an initial time with an initial guess of both flow and wall temperatures allows a solution of the new temperatures at each segment. Since the gas moves in a counter flow arrangement, however, the energy transferred to the wall is found using the temperature of the other gas at the previous timestep. This assumption is used until the calculation has proceeded over half the total tube length, in which case the new wall temperature has already been estimated. The heat capacities ($C_{1,hx}$,$C_{2,hx}$) and convective heat transfer coefficients of each fluid ($k_{1,hx}$,$k_{2,hx}$) are calculated using Cantera at each segment. The geometric dimensions and material constants are set to what is representative of a heat exchanger in an SOFC system. As these constants are not available in the literature, parameters are approximately matched to steady state data from commercially available fuel cell heat exchangers. Using the data in Table 3.2, with air for both fluids results in a steady state output shown in Figure 3.3. This result confirms the model predicts a reasonable steady state output.

3.4 Blowers

The blower model is implemented using a first principles model developed in Gelfi et al. [54]. The motor inertia is:

$$
\begin{aligned}
J\frac{d\omega}{dt} &= \tau_{motor} - \tau_{blo} \\
J\frac{d\omega}{dt} &= \frac{P_{motor}}{\omega} - \frac{P_{blo}}{\omega},
\end{aligned} \tag{3.14}
$$

where J is the blower inertia in kg/m^2, ω is the blower speed, τ_{motor} is the torque applied by the blower motor, τ_{blo} is the resistance torque of the blower, P_{motor} is the power applied by the motor, and P_{blo} is the power of the blower. An additional equation developing the change in pressure across the blower can also be used, however, Gelfi et al. [54] showed this to be significantly faster in response than the motor inertia. Thus the pressure is assumed

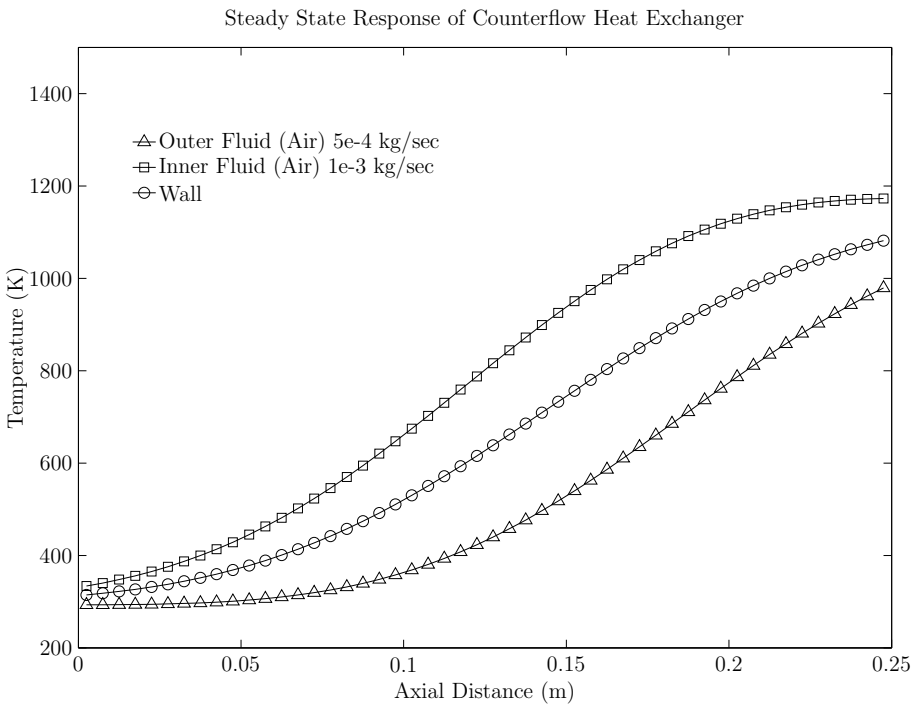

Figure 3.3: Heat Exchanger Steady State Response

to be steady state and is not used for the dynamic response of the blower over the time steps used. The blower power demanded is:

$$P_{blo} = C_{gas,blo}\frac{T_{env}}{\eta_{blo}}((\frac{p_{blo}}{p_{env}})^{\frac{\gamma-1}{\gamma}} - 1)\dot{m_{blo}} \tag{3.15}$$

The relationship between blower speed, mass flow, and efficiency is highly nonlinear and specific to the blower design. As in Gelfi et al. [54] this study makes use of an EBM centrifugal blower, model number DlG133-DC13-52. As with most commercial fans a blower map is available showing mass flow versus pressure differential generated (Figure 3.4). Three different voltages are represented in Figure 3.4. In order to solve the state equation in Eqn 3.14 the mass flow as a function of the motor speed and pressure differential is required. This function is done by performing a polynomial fit to the data points in Figure 3.4. The control signal for the blower is P_{motor}. Two blowers are present in the system, one for the air supply to the CPOX and one for the air supply to the stack. Fuel is assumed to be available at enough pressure that a third blower is not required. It should be noted that the same

		n [RPM]	P_1 [kW]	η_{tL} [%]	Lp_A [dBA]			n [RPM]	P_1 [kW]	η_{tL} [%]	Lp_A [dBA]
1	1'	1700	145	---	65	1	5	1400	78	---	60
1	2'	1930	133	38	62	1	6	1580	70	38	56
1	3'	2290	122	41	59	1	7	1760	56	41	53
1	4'	2700	99	32	61	1	8	2000	44	32	53
1	1	1580	118	---	64						
1	2	1790	107	38	61						
1	3	2100	95	41	57						
1	4	2410	73	32	58						

Curve

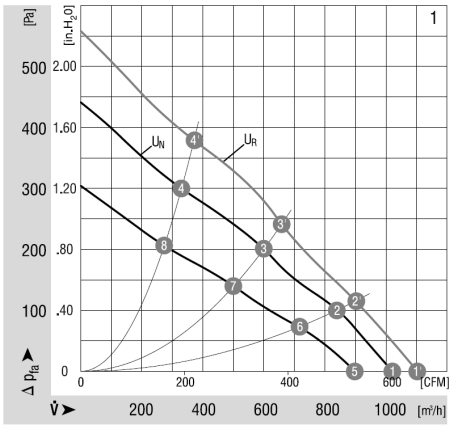

Figure 3.4: EBM Industries Blower Performance Map, taken from http://www.ebmpapst.us

blower is used for both air supplies, while the air supply to the stack requires a larger mass flow. Thus the blower to the reformer is oversized. Further improvements in efficiency and system response (at a cost of a reduced operating range) could be achieved with individual sized blowers.

3.5 Tail Gas Burner

The tail gas burner is used to preheat the system until the minimum operating temperature is reached, as well as use any extra fuel in the fuel stream to preheat the air for the SOFC stack. Cantera is well suited to modeling combustion processes, and is used to produce a transient burner model. The burner is modeled as an axisymmetric burner stabilized flame. This reduction results in a spatial one dimensional reacting flow model, which is solved over a spatial grid. The GRI30 reaction mechanism is used to calculate the reactions,

Table 3.2: SOFC System Physical Parameters

Parameter	Value
Fuel Reformer	
Inner Diameter	0.0082 m
Length	.0165 m
SOFC Stack	
Cell Outer Diameter	0.1 m
Cell Length	0.15 m
Heat Exchanger	
Wall Material	2205 stainless steel
HX Length	0.25 m
Inner Tube Diameter	0.025 m
Outer Tube Diameter	0.040 m
Wall Thickness	.005 m
Blowers	
Efficiency	0.38
Rotational Inertia	$4 \cdot 10^{-8}$ kg/m^2

3.6 Component Integration

All of the components above are interconnected with respect to mass flows and thermal effects. Transport systems must exist between components in order to move gas from the reformer to the stack and from the stack to the burner and heat exchanger. This piping will introduce mass flow delays and pressure losses into the system. Additional heat interactions will also occur during transport. These effects are mostly neglected within this thesis. Transport delays are considered in components with spatial models, specifically the SOFC stack and the heat exchanger. Other specific transport losses require knowledge of the system geometry and spacing of components. Since the system considered is a smaller 1.5 kilowatt system it is assumed components are closely spaced and transport heat losses and delays are small. As such they are neglected in this thesis, however, there will be significant heat interactions between components that are not modeled. The thermal effects between components will influence the operation of the system within constraints and producing models which capture these effects is a subject of further research.

3.7 Example System Response

An example response of the system model to increased current demand is shown in Figure 3.5. The voltage is dropped from 0.78 V to 0.69 V much faster than the timestep (0.1 seconds in Figure 3.5). The current increases, but initially the fuel utilization rate drops very low. One half second after the voltage drop the mass flow of fuel and air to the reformer and stack is increased, allowing the current to stabilize at the new demand. In addition to the fast voltage and current effects, the temperature response of the system is shown in Figure 3.6 for each of the considered components. The temperature response of the reformer is on the order of seconds, the stack is on the order of tens of seconds, and the heat exchanger is on the order of hundreds of seconds. These plots show the model is sufficient to predict the fast electrochemical response as well as the much slower thermal response of the system. They also illustrate the need for implementation of some form of control to avoid violating

constraints on the system.

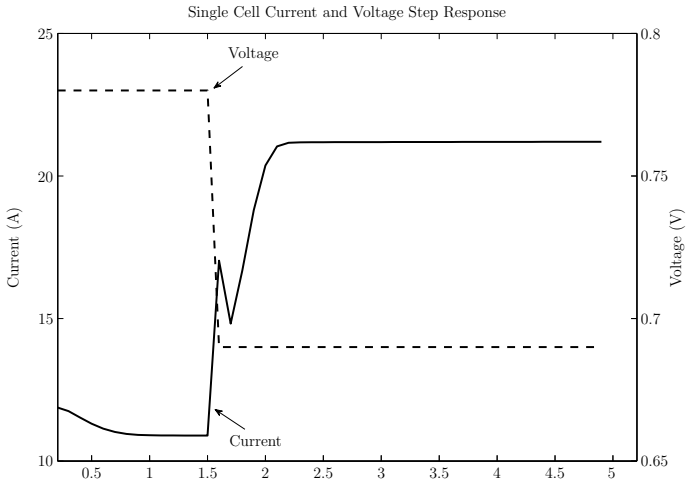

(a) Current and Voltage

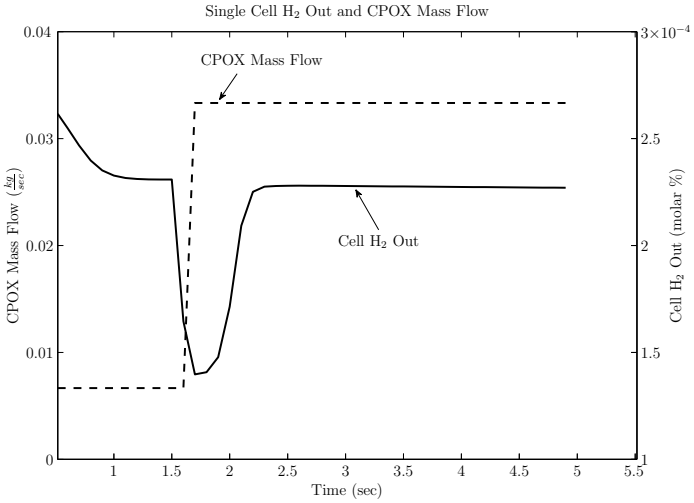

(b) Cell Mass Flow

Figure 3.5: System Step Response

3.8 System Constraints

Each of the system components listed in the previous sections have constraints on their operation. Limitations on temperature, composition, and mass flow vary for each of the components. For the CPOX reactor the composition constraints are also temperature dependent. The inclusion of these constraints into the control algorithm is a significant part of the research. The constraints in each BOP component and the system stack are discussed

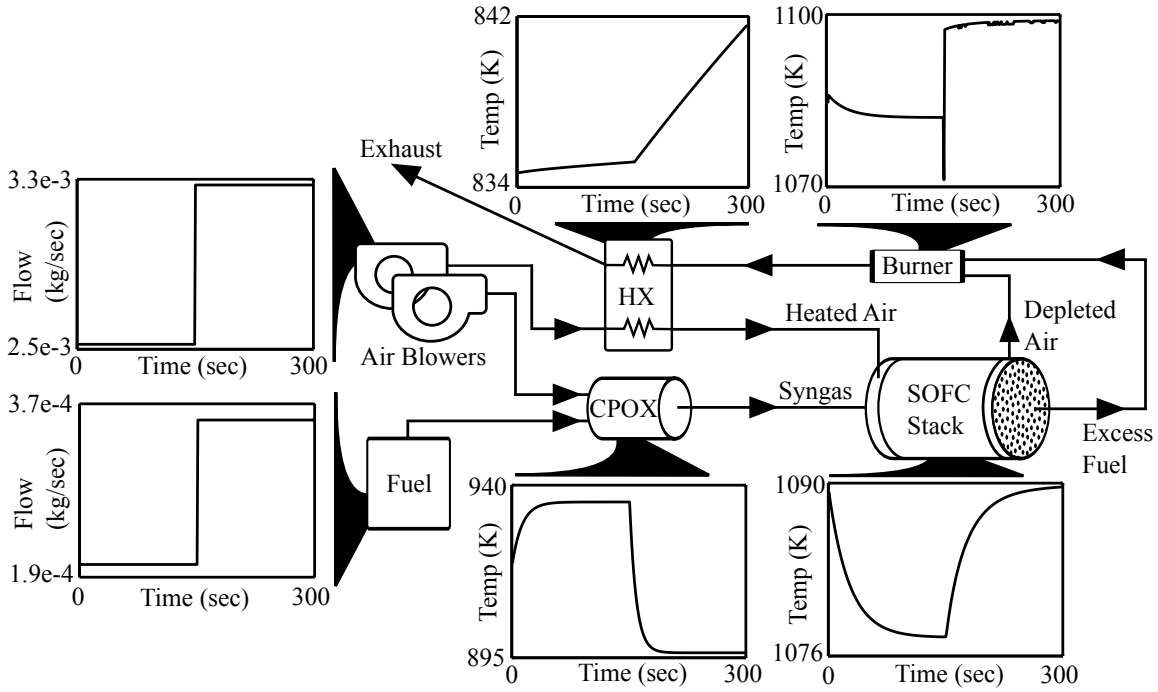

Figure 3.6: System components and temperature responses to step changes in air and fuel flows.

below.

3.8.1 SOFC Stack Constraints

The constraints on the SOFC stack include an adequate hydrogen supply in the outlet gas stream, as " cell starvation" can damage the stack. This constraint is usually enforced by fixing fuel utilization within the the controller. A more efficient (in terms of load following) method is to set a minimum percent of H_2 in the anode outlet and allow the controller to vary the fuel utilization subject to the constraint. Additionally the stack has a minimum and maximum operating temperature, as well as a maximum rate of temperature change. The allowable thermal gradient (both spatially and temporal) is a function of the stack geometry and material [55]. Our goal is to minimize the thermal gradient produced from any load changes, rather than set a hard limit on temperature changes, as little data exists on what gradients are allowable. The final constraint on the stack is that the outlet air stream contain enough oxygen to fully combust the remaining hydrogen in the tailgas burner. This

constraint ensures that there is no hydrogen present in the exhaust, as flammable exhaust is not desireable. Combustion of any remaining hydrogen also allows for a faster air pre-heat. The voltage of the stack is also a constraint, but as the system is modeled with voltage as an input, this constraint is considered an input limitation. Stack constraints on fuel composition are discussed in the next section.

3.8.2 CPOX Constraints

The reactor is limited by the sintering temperature of the catalyst. Since the CPOX reaction is exothermic, depending on the mass flow of the fuel, and the air fuel ratio, sufficiently high temperatures can be reached to completely destroy the catalyst within the reactor. The catalyst must also maintain a minimum operating temperature in order to avoid deactivation due to carbon deposition in the CPOX reactor. To avoid carbon deposition in the SOFC stack, the constraints are dependent on the outlet composition of the CPOX.

Early work on carbon deposition in fuel cells occurred in the 1960's with the calculation of equilibirum constants for the dominant carbon forming reactions and the representation of the carbon deposition barrier (CDB) on a ternary diagram [56, 57]. The impacts of biogas, and verification for ternary diagrams in avoiding carbon deposition is also demonstrated in Aravind et al. [58]. Calculation of fuel maps to statically determine optimal SOFC fuel composition with respect to efficiency and voltage have been demonstrated as well [59, 60]. This thesis uses the method in Farhad and Hamdullahpur [59, 60] dynamically within the CPOX model to determine the distance of a fuel composition from the CDB. In order to ensure that carbon deposition does not occur in the SOFC stack, the variables of concern are the temperature and outlet composition of the CPOX. The partial pressures are normalized with respect to any inert gas in the composition and the three CHO coordinates plotted as:

$$
\begin{aligned}
\mathrm{C} &= \frac{x_{\mathrm{CO_2}} + x_{\mathrm{CH_4}} + x_{\mathrm{CO}}}{2x_{\mathrm{H_2}} + 3x_{\mathrm{CO_2}} + 2x_{\mathrm{CO}} + 3x_{\mathrm{H_2O}} + 5x_{\mathrm{CH_4}}} \\
\mathrm{H} &= \frac{2x_{\mathrm{H_2}} + 2x_{\mathrm{H_2O}} + 4x_{\mathrm{CH_4}}}{2x_{\mathrm{H_2}} + 3x_{\mathrm{CO_2}} + 2x_{\mathrm{CO}} + 3x_{\mathrm{H_2O}} + 5x_{\mathrm{CH_4}}} \\
\mathrm{O} &= \frac{2x_{\mathrm{CO_2}} + x_{\mathrm{CO}} + x_{\mathrm{H_2O}}}{2x_{\mathrm{H_2}} + 3x_{\mathrm{CO_2}} + 2x_{\mathrm{CO}} + 3x_{\mathrm{H_2O}} + 5x_{\mathrm{CH_4}}}
\end{aligned}
\tag{3.16}
$$

where x_j is the fraction of species j. To calculate if solid carbon can form, three reactions are considered:

$$
\begin{gathered}
\mathrm{CH_4} \leftrightarrow \mathrm{C} + 2\mathrm{H_2} \\
\mathrm{H_2} + 2\mathrm{CO} \leftrightarrow \mathrm{C} + \mathrm{H_20} \\
2\mathrm{CO} \leftrightarrow \mathrm{C} + \mathrm{CO_2}
\end{gathered}
\tag{3.17}
$$

The species partial pressures in Equation 3.17 require the estimation of the outlet composition of the CPOX at each time step. Calculation of the CDB requires the estimation of the CPOX reformate outlet temperature at each time step. The CPOX model provides the outlet temperature from which the equilibrium constants for each of the reactions in equation 3.17 can be calculated using the Gibbs energy of each non-inert gas constituent. Setting the net carbon produced to zero and sweeping the value of either C,H, or O from 0 to 100 calculates the percentage of the other two along the CDB at the current temperature. At each model timestep, the CPOX outlet gas temperature is calculated, and a new CDB is found, as well as the distance (in ternary space) between the current composition and the point at which solid carbon can form. In order to find the distance to the CDB, a cartesian mapping is applied to the ternary coordinates. No information is lost, as the third coordinate in the ternary space is dependent on the other two. The cartesian mapping takes the HO axis of the ternary diagram as the x-axis of a 2 dimensional cartesian space. The (x, y) coordinates can then be found for both the reformate composition and the CDB using:

$$
(x, y) = \left(\frac{2O + C}{2(H + O + C)}, \frac{\sqrt{3}C}{2(H + O + C)} \right). \tag{3.18}
$$

The CDB distance is then the difference in the y coordinate between the reformate composition and the CDB line at the x coordinate of the reformate composition. Since the CDB is only available as discrete data points, cubic spline interpolation is used to determine the

y coordinate of the CDB at the x coordinate of the reformate, utilizing all available data points. The two are then subtracted to determine the CDB distance. This distance becomes a constraint in the MPC control algorithm.

This analysis is based solely off equilibrium chemistry and does not consider the material properties of the cell. The provided measure of carbon formation is not intended to replace a detailed kinetic analysis. It is not a useful measure to determine what cell geometries, temperature, and compositions contribute to solid carbon formation. However, since the object is to control the reformate composition it provides a measure of "reformate quality" as far as carbon deposition, which has mostly been ignored in previous SOFC system control methods. Previous control methods have fixed the oxygen to carbon ratio to avoid carbon deposition. The use of the CDB distance measure considers the current temperature in addition to the $\frac{O_2}{CH_4}$ ratio and allows for greater freedom in choosing operating points to meet load following demands. An example fuel reformate is plotted for 894.76 K along with the corresponding CDB in Figure 3.7. This composition is below the CDB so it is not prone to carbon formation and represents an acceptable reformate composition for use in the stack.

3.8.3 Other BOP Constraints

The blowers used provide some constraints to the system as they have a maximum mass flow that can be obtained for a given pressure as well as a power limit that can be fed to the blower motors. These are both function of the chosen blower and are non-varying constraints. The burner and heat exchanger do not add any constraints to the control algorithms, only to the dynamic response of the system.

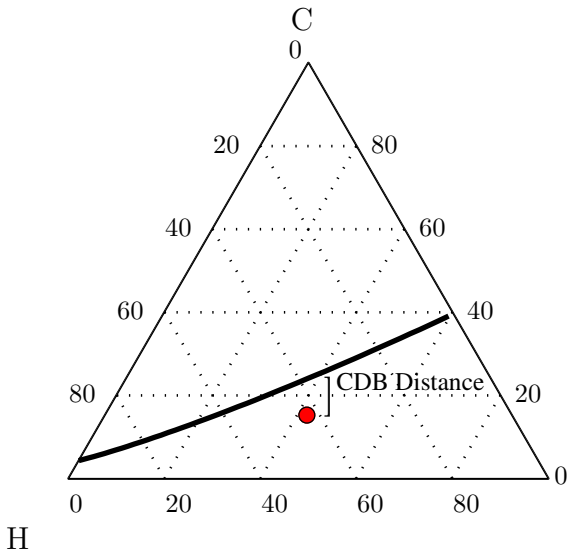

Figure 3.7: Fuel Ternary Diagram, CDB for 894.76 K (black), reformate composition with inlet $\frac{O_2}{CH_4} = 1.97$ (red).

CHAPTER 4

SYSTEM REDUCTION AND CONTROL

The nonlinear model developed in the previous chapter does not perfectly match any existing physical system. There are also many unknown constants which can never be measured to create a "perfect" model. Both the nonlinear model and the LPV model outputs will not equal the plant outputs for a given set of inputs and initial conditions. This inaccuracy does not mean the models are not useful, however. As long as the models can capture some of the dynamics of the system, they can be used in robust MPC algorithms which outperform feedback control algorithms that do not utilize a plant model. The goal of system reduction is to take a highly complex nonlinear model and reduce the parameter space to a much lower order, allowing for on-line (real-time) calculation of the desired control inputs. Although the reduction of the nonlinear model does result in error, the use of a scheduled LPV implementation ensures the reduced model captures the system dynamics over a very wide range of operating conditions.

4.1 System Model Reduction

System reduction via system identification is a technique to identify a low order dynamic model using experimental data. For the previously described SOFC model, the system is described by a large number of non-linear differential and algebraic differential equations. Model evaluations can take on the order of a minute for large changes in system state. Although this model is easily accurate enough for control purposes, the non-linearity and evaluation time make it unsuitable for use in a model predictive controller. Ideally a single linear model could be found that would allow for a fast optimal control of the system, however, due to the large non-linearities present over the operating range, no such model exists. Thus a linear parameter varying (LPV) model that is a combination of linear models which are blended based on a signal is chosen to represent the SOFC system.

Several approaches in the field of system identification work to solve this problem. Subspace LPV identification was chosen as it creates a state space model, suitable for model predictive control. Subspace LPV identification algorithms can be divided into two approaches, local and global. Local approaches find linear models around operating points and interpolate between them using a function of a measured quantity. Global approaches attempt to excite all desired non-linearities in the system in a single experiment, and then fit the model based on a functional dependence to one or more measured quantities.

We use a LPV global approach to the identification problem, described in detail in van Wingerden and Verhaegen [61] and implemented in Houtzager et al. [62]. The model structure is given in Eq.(4.1), where $x_k \in \mathbb{R}^n$ is the state at time k and system matrices are $A^{(i)} \in \mathbb{R}^{n\times n}$, $B^{(i)} \in \mathbb{R}^{n\times r}$, $K^{(i)} \in \mathbb{R}^{n\times l}$ for $i = \{1...m\}$, along with $C \in \mathbb{R}^{l\times n}$, and $D \in \mathbb{R}^{l\times r}$. The described system has inputs $u_k \in \mathbb{R}^{r\times 1}$, and outputs $y_k \in \mathbb{R}^{l\times 1}$. $\mu \in \mathbb{R}^{m\times L}$ is a scheduling variable which determines how the m different linear models are combined at each of the L timesteps. e_k is an unmeasured disturbance. The unmeasured disturbance acts as an innovation to the state at each timestep, through K.

$$\begin{aligned} x_{k+1} &= \sum_{i=1}^{m} \mu_k^{(i)}(A^{(i)}x_k + B^{(i)}u_k + K^{(i)}e_k) \\ y_k &= Cx_k + Du_k + e_k. \end{aligned} \tag{4.1}$$

For the SOFC system analyzed, model inputs that are components of u are the reformer blower command (p_{blo}), the stack blower (p_{stack}) command, fuel mass flow to the reformer (m_{fuel}), and the stack voltage (V). Outputs that are components of y are the variables that require regulation or are need to impose constraints. These are taken as the current (I), the MEA assembly temperature (T_{MEA}), the hydrogen exhaust concentration and the temperature of the gas exiting the fuel reformer (T).

The algorithm reconstructs a valid state sequence using the known input and output data as well as the presumed scheduling sequence. Once this is done the unknown system matrices ($A^{(i)}$, $B^{(i)}$, $K^{(i)}$, C, D, for $i = \{1...m\}$) are found via least squares. To explain how this calculation is done, the model is rewritten in predictor form:

$$
\begin{aligned}
x_{k+1} &= \sum_{i=1}^{m} \mu_k^{(i)} (\tilde{A}^{(i)} x_k + \tilde{B}^{(i)} u_k + K^{(i)} y_k) \\
&\text{where} \\
\tilde{A}^{(i)} &= A^{(i)} - K^{(i)} C \\
\tilde{B}^{(i)} &= B^{(i)} - K^{(i)} D.
\end{aligned} \tag{4.2}
$$

The input/output data is also vectorized, and combined sequentially into length p windows, denoted by $\bar{z}_k^p$:

$$
\begin{aligned}
z_k &= \begin{bmatrix} u_k^T & y_k^T \end{bmatrix}^T \\
\bar{z}_k^p &= \begin{bmatrix} z_k \\ z_{k+1} \\ \vdots \\ z_{k+p-1} \end{bmatrix}.
\end{aligned} \tag{4.3}
$$

The window size (p) determines the block size over which the system states are estimated, and thus has a large influence on the size of the resulting problem. Thus for an example problem with $p = 2$, there are $\{N - p\}$ $\bar{z}_k^p$ matrices constructed as:

$$
\bar{z}_k^p = \begin{bmatrix} u_k \\ y_k \\ u_{k+1} \\ y_{k+1} \end{bmatrix}. \tag{4.4}
$$

The effect of the window size is discussed later in this chapter. For future use we define the quantities

$$
\begin{aligned}
\phi_{j,k} &= \tilde{A}_{k+j-1} ... \tilde{A}_{k+1} \tilde{A}_k, \\
L_1 &= \begin{bmatrix} \bar{B}^{(1)} & ... & \bar{B}^{(m)} \end{bmatrix}, \\
L_j &= \begin{bmatrix} \tilde{A}^{(1)} L_{j-1} & ... & \tilde{A}^{(m)} L_{j-1} \end{bmatrix}, \\
K^p &= \begin{bmatrix} L_p & L_{p-1} & ... & L_1 \end{bmatrix},
\end{aligned} \tag{4.5}
$$

where:

$$
\tilde{A}_k = \sum_{i=1}^{m} \mu_k^{(i)} (\tilde{A}^{(i)}) \tag{4.6}
$$

and

$$
\bar{B}^{(i)} = \begin{bmatrix} \tilde{B}^{(i)} & K^{(i)} \end{bmatrix}. \tag{4.7}
$$

Also define the following functions of the scheduling sequence (μ), which make use of the kronecker product ($\otimes$):[1]

$$\begin{aligned} P_{p|k} &= \mu_{k+p-1} \otimes ... \otimes \mu_k \otimes I_{r+l} \\ N_k^p &= \begin{bmatrix} P_{p|k} & & & 0 \\ & P_{p-1|k+1} & & \\ & & \ddots & \\ 0 & & & P_{1|k+p-1}. \end{bmatrix} \end{aligned} \tag{4.8}$$

The state and output p time steps in the future can be written as:

$$\begin{aligned} x_{k+p} &= \phi_{p,k} x_k + K^p N_k^p \bar{z}_k^p \\ y_{k+p} &= C(\phi_{p,k} x_k + K^p N_k^p \bar{z}_k^p) + D u_{k+p}. \end{aligned} \tag{4.9}$$

In order to reconstruct a basis for the state sequence, the state transition matrix is assumed to be zero outside each length p time window. This assumption is based on the idea that the system is stable, so for a suitably large p, the influence of x_k on $x_k + p$ is small. Thus $\phi_{j,k} = 0$ for all $j \geq p$. Using a small p introduces a bias into the estimate, as p increases the approximation bias decreases. This key assumption allows for the decompostion, and thus estimation of the state (from the matrix $K^p N_k^p \bar{z}_k^p$). Using this approximation the state sequence and known outputs are:

$$\begin{aligned} x_{k+p} &= K^p N_k^p \bar{z}_k^p \\ y_{k+p} &= C K^p N_k^p \bar{z}_k^p + D u_{k+p}. \end{aligned} \tag{4.10}$$

Extended input and output matrices are then stacked over all windows of length p available from the identification data set. Define

$$\begin{aligned} U &= \begin{bmatrix} u_{p+1} & ... & u_n \end{bmatrix}, & Y &= \begin{bmatrix} y_{p+1} & ... & y_n \end{bmatrix}, \\ Z &= \begin{bmatrix} N_1^p \bar{z}_1^p & ... & N_{N-p+1}^p \bar{z}_{N-p+1}^p \end{bmatrix}, & X &= \begin{bmatrix} x_{p+1} & ... & x_N \end{bmatrix}. \end{aligned} \tag{4.11}$$

The matrices D and CK^p can then be found by solving the following minimization problem:

$$\min_{CK^p, D} \|Y - CK^p Z - DU\|_F^2. \tag{4.12}$$

[1]The kronecker product is an operation for creating block matrices from arbitrary size input matrices. It is defined as:

$$A \otimes B = \begin{bmatrix} a_{1,1}B & \cdots & a_{1,n}B \\ \vdots & \ddots & \vdots \\ a_{m,1}B & \cdots & a_{m,n}B \end{bmatrix}$$

Under the assumption in (4.10), the state sequence X is equal to K^pZ. However, the minimization problem in (4.12) provides an estimate of CK^p. Define the extended observability matrix Γ^p:

$$\Gamma^p = \begin{bmatrix} C \\ C\tilde{A}^{(1)} \\ \vdots \\ C\tilde{A}^{(1)^{p-1}} \end{bmatrix}. \tag{4.13}$$

Then following from (4.10):

$$\Gamma^p K^p Z = \Gamma^p X, \tag{4.14}$$

and we can utilize the product of $\Gamma^p K^p$ and the known Z matrix to find the state sequence. The matrix $\Gamma^p K^p$ is the product of the extended controllability and observability matrix. In order to build $\Gamma^p K^p$, utilize the structure of the already estimated CK^p (found from (4.12)):

$$\begin{aligned} CK^p &= \begin{bmatrix} CL_p & CL_{p-1} & \cdots & CL_1 \end{bmatrix}, \\ CL_p &= \begin{bmatrix} C\tilde{A}^{(1)}L_{p-1} & \cdots & C\tilde{A}^{(m)}L_{p-1} \end{bmatrix}, \\ \Gamma^p K^p &= \begin{bmatrix} CL_p & CL_{p-1} & \cdots & CL_1 \\ 0 & C\tilde{A}^{(1)}L_{p-1} & \cdots & C\tilde{A}^{(1)}L_1 \\ 0 & & \ddots & \\ 0 & & & C\tilde{A}^{(p-1)}L_1. \end{bmatrix} \end{aligned} \tag{4.15}$$

Thus the rows of $\Gamma^p K^p$ are made up of shifted block elements of the already estimated CK^p. Explicitly writing these blocks for CK^p:

$$CK^p = \begin{bmatrix} \begin{bmatrix} C\tilde{A}^{(1)}L_{p-1} & \cdots & C\tilde{A}^{(m)}L_{p-1} \end{bmatrix} & \cdots & \begin{bmatrix} C\tilde{A}^1L_0 & \cdots C\tilde{A}^{(m)}L_0 \end{bmatrix} \end{bmatrix} \tag{4.16}$$

The first row of $\Gamma^p K^p$ is taken as the matrix CK^p and additional rows are built using selected blocks corresponding to the proper value of p.

In order to find the state sequence, a singular value decomposition (SVD) is used:

$$\Gamma^p K^p Z = \begin{bmatrix} U & U_\perp \end{bmatrix} \begin{bmatrix} \Sigma_n & 0 \\ 0 & \Sigma \end{bmatrix} \begin{bmatrix} V \\ V_\perp \end{bmatrix}, \quad \hat{X} = \Sigma_n V. \tag{4.17}$$

The state sequence is the product of Σ_n and V. The state size is determined by detecting a gap between the magnitude of the singular values. In practice the size of this problem grows very quickly. The matrix Z needs to be decomposed, which has number of rows equal to:

$$\rho_Z = (r+l)\sum_{j=1}^{p} m^j. \tag{4.18}$$

This term rapidly outstrips the memory available in most desktop computers, even for small systems. In order to remain feasable a more efficient method is required. To that end, the Lagrangian dual problem of (4.12) can be solved with respect to the minimum norm solution:

$$\min_{\alpha} \|\alpha\|_F^2 \quad s.t. \quad Y - \alpha(Z^T Z + U^T U) = 0. \tag{4.19}$$

The Lagrangian dual problem adds the constraints to the objective function, and then minimizes the Lagrange variable ($\alpha \in \mathbb{R}^{l \times N-p-1}$). Thus $\alpha = Y[Z^T Z + U^T U]^{-1}$ and an estimate of CK^pZ is given by:

$$C\hat{K}^p Z = \alpha Z^T Z \tag{4.20}$$

Additionally the matrix $\Gamma^P K^P Z$ is found as

$$\Gamma^P K^P Z = \begin{bmatrix} \alpha \sum_{j=1}^{p} (Z^{1j})^T Z^{1j} \\ \alpha \sum_{j=2}^{p} (Z^{2j})^T Z^{2j} \\ \vdots \\ \alpha \sum_{j=p}^{p} (Z^{pj})^T Z^{pj} \end{bmatrix}, \tag{4.21}$$

where

$$Z^{ij} = \begin{bmatrix} P_{p-j+1|j-i+1} z_{j-i+1} & \cdots & P_{p-j+1|N-p+1-i+1} z_{N-p+1-i+1} \end{bmatrix}. \tag{4.22}$$

This method avoids storing the large Z matrix, only the much smaller $Z^T Z$ matrix is needed. This matrix is square with size equal to the number of data points. The only matrices that need to be explicitly calculated are thus $(Z^{ij})^T Z^{ij}$. Where

$$\alpha Z^T Z = \alpha \sum_{j=1}^{p} (Z^{1j})^T Z^{1j}. \tag{4.23}$$

The matrix $Z^T Z$ is also almost always ill-conditioned, so Tikhonov regularization is used in the solution of (4.19). Tikhonov regulation attempts to weight a property of the solution (such as its 2-norm) to compensate for a poorly conditioned problem. Using regularization, the following is solved for α:

$$\min_{\alpha}(\|Y - \alpha(Z^T Z + U^T U)\|_F^2 + \lambda^2 \|\alpha\|_F^2. \tag{4.24}$$

The weighting λ can be set to identity.

Once the state sequence is found, least squares is used to estimate the remaining system matrices ($A^{(i)}$,$B^{(i)}$ for $i = \{1..m\}$). The determination of the system matrices is a two step procedure using the estimated state sequence and the known scheduling sequence, input and outputs. Initially, the C and D matrices are estimated to minimize the residual e_k via the following regression problem:

$$e_k = y_k - (Cx_k + Du_k) \tag{4.25}$$

The $A^{(i)}$, $B^{(i)}$, and $K^{(i)}$ matrices are found by using the scheduling relationship (shown only for A, but holds for both $A^{(i)}$, $B^{(i)}$, and $K^{(i)}$):

$$\left[\begin{bmatrix}\mu_0^T \\ \vdots \\ \mu_k^T\end{bmatrix} \otimes I_{n,n}\right] \begin{bmatrix}A^1 \\ \vdots \\ A^m\end{bmatrix} = \begin{bmatrix}A_1 \\ \vdots \\ A_N\end{bmatrix}. \tag{4.26}$$

This relationship is then substituted into the state space equation:

$$x_{k+1} = A_k x_k + B_k u_k + K_k e_k. \tag{4.27}$$

$A^{(i)}$, $B^{(i)}$ and $K^{(i)}$ appear linearly in Eq. (4.27), thus given x, u, and e, they can be solved for using least squares. The resulting $N-1$ equations, are solved for the unknown time varying system matrices. The LPV system matrices are then directly calculated from the scheduling part of (4.26). This operation requires a well conditioned scheduling sequence to find a useful set of system matrices. Proper scaling of the scheduling sequence is thus required to ensure a well conditioned result. Since different physical quantities are being measured and incorporated into the scheduling sequence (in this case, the current and MEA temperature), each needs to be consistently scaled to obtain singular values of similar magnitude. The scaling also needs to be pre-determined, as the the scaling used in the identification experiment must match that used in any validation data. This scaling then becomes a problem of ensuring that all the measured components of the scheduling sequence vary over their entire

anticipated range during the identification experiment. Experimentally it was found that a condition number above 40 does not produce a useable model. It should be noted that since only a basis was found for the state sequence in Eq. (4.17), the system matrices found can only be accurate up to a transform.

The LPV identification algorithm depends on the existence and measurability of a scheduling parameter (μ), which forms the system matrices at each time step according to (4.2). The choice of scheduling parameter has a strong impact on the accuracy of the identified model. Ideally, physical intuition could be used to separate the system into linear modes using a measured variable. However in the case of an SOFC system the dynamics depend on too many variables, some of which may not be measurable to easily schedule the system. The stack current has been used as the scheduling parameter in previous stack identification and control applications [37]. However, current does not provide a perfect scheduling parameter. There are a multitude of operating points with large variations in reformate composition, mass flow, and voltage, that all produce the same current. It is part of the control challenge to choose amongst these operating conditions. As such, utilizing only current as a scheduling variable is limiting, however, additional measurements are often available. The temperature of the stack MEA can be used as a measurement, as well as the temperature of the reformate gas leaving the fuel reformer. These additional measurements can provide additional components for the scheduling sequence. Indeed, previous work has shown that the inlet composition of the fuel to the reformer can be estimated using only the reformate temperature as a measurement [47]. Whatever the choice of parameter, normalization and conditioning of the scheduling sequence is critical, as an ill-conditioned scheduling sequence results in an ill conditioned Z due to the large number of Kronecker products involved in its construction (Eq. 4.8). The scheduling sequence must also be inverted to find the system matrices after the state sequence is estimated (Eq. 4.26). For the developed SOFC model and the scheduling parameters tested, increasing the number of models generally results in a decreased condition number for the scheduling sequence, which causes numerical instabilities

before the curse of dimensionality renders the problem intractable.

When the identification procedure is implemented, variables to be chosen include the scheduling parameter (μ), the number of linear models to blend (m), the time window (p), and the dimension of the resulting models (n). Results for various combinations of these parameters are presented later within the results chapter. The range of operating conditions over which the identification experiment is simulated must also match the desired operating regions of the system. The identification data set was chosen to cover as wide a range as possible; approximately 0 to 25 amperes/cell, with both large mass flow and low mass flow conditions represented, as well as jumps between them. Identification and validation experiments are plotted within a reduced parameter space in Figure 4.1. This plot represents the parameter space using three parameters which are combinations of the selected inputs and the output that we desire to regulate. The ratio of fuel and air fed to the reformer is shown using the $\frac{O_2}{CH_4}$ ratio. The total mass flow of fuel and air to both the stack and the blower and the current are also shown. Using this parameter space it can be seen that the identification experiment is representative of the expected operating conditions. The identified data points are clustered around the steady state operating conditions represented by the red boxes. If the desired operating condition is not close to any of the identified points, we would expect the LPV model to be a poor fit. This reduced parameter space does not take into account voltage or indicate which operating conditions would violate system constraints. It does, however, allow for a visualization of the identification experiment relative to the desired operating conditions. For each operating condition, PRBS perturbations are added; example inputs used are shown in Figure 4.2. Several operating points, from high to low current with varying mass flows and $\frac{O_2}{CH_4}$ ratios are chosen. The magnitude of the PRBS perturbations is then set to induce output changes around that operating point.

4.2 Model Predictive Control

Model predictive control has been applied to SOFC systems previously [38, 39, 63] but not with a model of sufficient fidelity to estimate fuel composition throughout all compo-

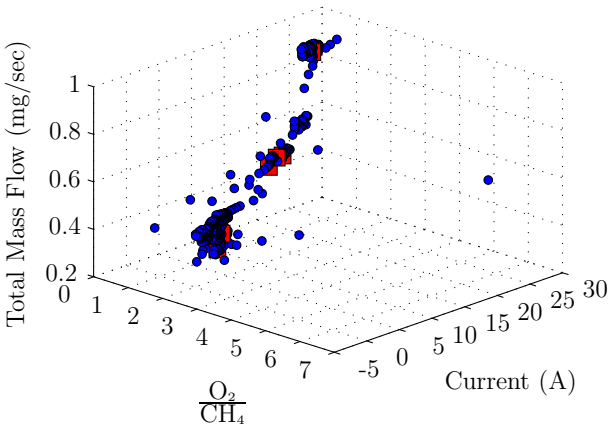

Figure 4.1: Identification and validation parameter space , the validation data set is shown using red squares. The identification data set is shown using blue circles.

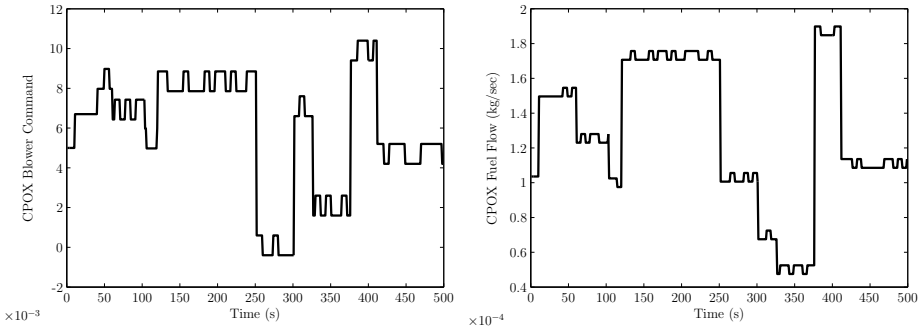

(a) Reformer Blower Command (b) Reformer Fuel Flow

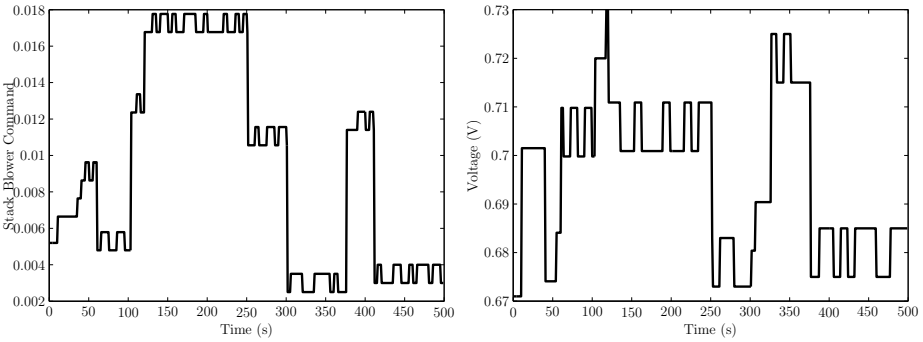

(c) Stack Blower Command (d) Voltage

Figure 4.2: Inputs used for identification experiment.

nents in the system. The use of an LPV model allows for linear MPC to be applied where previous work has resorted to nonlinear MPC implementations. With the development of a sufficiently detailed system level model, carbon formation can be avoided and temperature limits maintained while still allowing load following. The controller signal flow diagram is shown in Figure 4.3. The measurable outputs are taken from the SOFC system at each

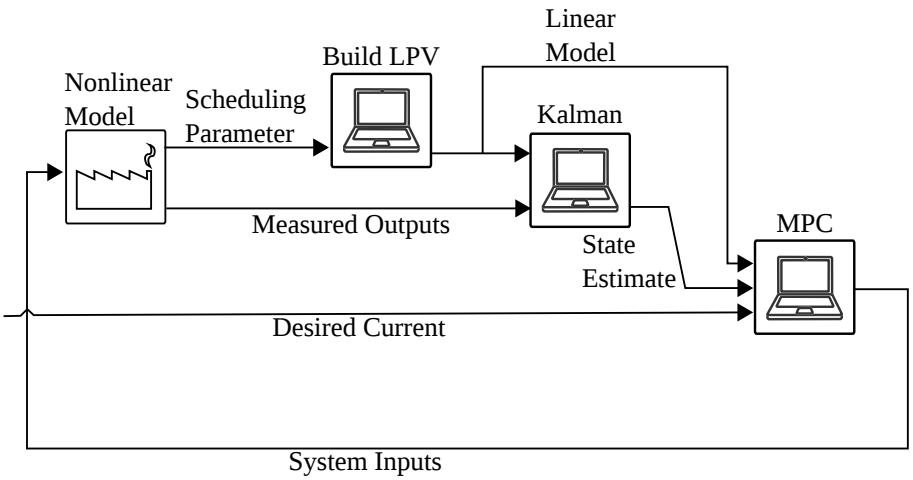

Figure 4.3: MPC Process Flow

time step. The scheduling sequence is calculated from the measured outputs and used to calculate the current linear model using the LPV framework (Eq. 4.10), this corresponds to finding the model at the current operating point. This linear model is then used within a standard Kalman filter (along with the measurements) to obtain a full state estimate. The Kalman filter recursively estimates the state of a process by utilizing a model of that process and measurements from the actual process. By combining knowledge of the covariance of the noise present in the measurements and the noise present in the process, it produces an estimate that minimizes the mean of the squared error between the estimate and the actual states. The Kalman filter operates in two steps, initially the state estimate is projected ahead in time, and second, the measurements are used to adjust the projected states. The first step uses the model and is as follows:

$$\begin{aligned} \hat{x}_k^- &= A_k \hat{x}_{k-1} + B_k u_{k-1} \\ P_k^- &= A P_{k-1} A^T + Q \end{aligned} \tag{4.28}$$

The new estimate of the state before the measurement update ($\hat{x}_k^-$) is calculated using the system model state space matrices (A_k, B_k) and the previously estimated state ($\hat{x}_{k-1}$) and the known input (u_{k-1}). The pre-measurement state estimate covariance (P_k^-) is also calculated. The state estimate and covariance are then updated to reflect information from the measurement:

$$\begin{aligned} K_k &= P_k^- C_k^T (C_k P_k^- C_k^T + R)^{-1} \\ \hat{x}_k &= \hat{x}_k^- + K_k (z_k - (C_k \hat{x}_k^- + D u_k)) \\ P_k &= (I - K_k C_k) P_k^- \end{aligned} \tag{4.29}$$

The first line in Eq. (4.29) calculates the Kalman gain (K_k) which determines the weight of the new measurement using the measurement error covariance (R), the system matrix C_k and the pre-measurement state estimate covariance. Once the gain is found, the state estimate ($\hat{x}_k$) is updated using the gain and the difference between the actual measurement (z_k) and the expected measurement ($C\hat{x}_k^- + Du_k$). Finally the state estimate covariance is updated. The measurements used for the Kalman filter include the current, the MEA temperature, and the reformate temperature. Thus only the corresponding rows of the identified C_k matrix are used to produce a full state estimate. With an estimate for these two quantities in hand, the model at the current time-step calculated and the desired current, the standard MPC optimization problem can be solved over a time window of N samples. The full identified C_k is used within the MPC algorithm to predict the two unmeasurable quantities we are interested in (H_2 exhaust and the CDB distance). The resulting quadratic cost optimization problem (Eq. (4.30)) gives the inputs to be applied at the next time-step.

$$
\begin{aligned}
J = \underset{u}{\text{minimize}} \quad & \sum_{i=0}^{N-1} x_{k,i}^T Q x_{k,i} + u_{k,i}^T R u_{k,i} + \parallel Q_Y(y_{k,i} - y_{ref,i}) \parallel_2 \\
\text{subject to} \quad & y_{k,i}(1) \leq 1200, \ i = 0, \ldots, N-1 \\
& y_{k,i}(3) \geq .025, \ i = 0, \ldots, N-1 \\
& 650 \leq y_{k,i}(4) \leq 1075, \ i = 0, \ldots, N-1 \\
& y_{k,i}(5) > 0, \ i = 0, \ldots, N-1 \\
& .675 \leq u_{k,i}(4) \leq .725, \ i = 0, \ldots, N-1 \\
& x_{k,i+1} = A_k x_{k,i} + B_k u_{k,i} \\
& y_{k,i} = C x_{k,i} + D u_{k,i} \\
& x_{k,N} \in \chi
\end{aligned}
\tag{4.30}
$$

Note that variables are as defined in Eq (4.1) and (1.6). A tracking implementation with a $N = 7$ step horizon is implemented with output weights only on the current, exhaust $H_2\%$ and the CDB distance. The demand current, target exhaust $H_2\%$ and target CDB distance are considered static over the horizon $(1...N)$ for the optimization problem in Eq 4.30. They are also updated at every timestep after applying the calculated inputs. The double index indicates what variables are constant over the horizon i, yet change at every timestep, k. The use of parenthesis indicate an index, thus $u_{k,i}(4)$ indicates the fourth input at timestep k and horizon i. The weighting for the current is five orders of magnitude larger than that of the exhaust $H_2\%$ and CDB distance. This weighting has the effect of primarily ensuring the demand current is met. The smaller weights push the controller to keep the exhaust $H_2\%$ and CDB distance above their hard constraint minimums. This stabilization is to account for modeling error, forcing the controller to operate at some distance from the hard constraints. The state and input weights are both set to identity as the only requirement is to stay within hard constraints. In order to enforce stability, a terminal set (χ) is computed within the controller. This constraint limits the size of the controllable state for a finite horizon, but does guarantee stability [64]. All weights are summarized in Table 4.1.

Table 4.1: MPC Weights

Parameter	Value
Q_Y	$\begin{bmatrix} 0 & 0 & 0 & 0 & 0 \\ 0 & 10^5 & 0 & 0 & 0 \\ 0 & 0 & 1.0 & 0 & 0 \\ 0 & 0 & 0 & 0 & 0 \\ 0 & 0 & 0 & 0 & 1.0 \end{bmatrix}$
R	$\begin{bmatrix} 1 & 0 & 0 & 0 \\ 0 & 1 & 0 & 0 \\ 0 & 0 & 1 & 0 \\ 0 & 0 & 0 & 1 \end{bmatrix}$
Q	$\begin{bmatrix} 1 & 0 & 0 & 0 & 0 \\ 0 & 1 & 0 & 0 & 0 \\ 0 & 0 & 1 & 0 & 0 \\ 0 & 0 & 0 & 1 & 0 \\ 0 & 0 & 0 & 0 & 1 \end{bmatrix}$

4.3 Rate Limited MPC

The MPC optimization problem faces two challenges to determining useful inputs. First are the errors between the actual system and the LPV model used to control it. Second, are the changing model dynamics over the optimization window. If the model dynamics change too much the MPC controller cannot predict the outputs for a calculated input. Thus constraints can be violated and the operational setpoints missed.

Approaches to accounting for the LPV model mismatch include the use of MPC algorithms that incorporate the changing LPV dynamics. This can be done by solving a min/max optimization problem taking into account a worst case bound on the scheduling variable. Recent examples of this approach have been developed and tested on small single input systems ([65], [66]). Solving for an explicit controller over a range of models is challenging from a computational standpoint. Computations times for higher order multiple input systems are still prohibitive to calculate. The use of the identified seven state, four input, five output model proved too challenging from a computational perspective to implement and explicit LPV/MPC controller.

Ideally the scheduling sequence would be known beforehand. In this case the MPC control problem would be reduced to implementing MPC on a linear time varying system. Although computationally more challenging than standard MPC, efficient implementations exist ([67]). In our case, the actual scheduling variable is unknown as it is the output of the non-linear system or the actual plant. What is available is the MPC predicted estimate of the output over the prediction horizon. This information could be used to iteratively calculate a time varying set of models which could be used in MPC. This approach is currently being pursued as a future topic of research.

As some method to rate limit the reference current is needed, this section details an easily implemented approximate technique motivated by robust control theory. We represent the changing dynamics as a possible set of models ($\wp$). If the LPV model is scheduled using the combination of the current and MEA temperature measurements, then $\wp$ consists of all the models produced by all the possible current and temperature combinations. We desire the MPC algorithm to be stable for all models within the set $\wp$. Calculation of the entire set $\wp$ is infeasible. However, we can represent the LPV model at the desired current as a nominal model, and look at the perturbation between this nominal model and the LPV model calculated using the measurements at the current time step. Simulating over a range of operating conditions allows us to build up an expected perturbation for a set of current magnitude changes. Then using the expected disturbance we can limit the current magnitude change to ensure a controller is stable to all models within the expected disturbance.

Before calculating the expected perturbation for a set of current magnitude changes, we must define how that disturbance acts on the nominal model. Define a perturbed model transfer function ($\tilde{P}$) using a multiplicative disturbance transfer function (W), and the nominal model (the dynamics at the desired current) such that:

$$\tilde{P} = (1 + W)P_{nom}. \tag{4.31}$$

The perturbation W is then defined such that:

$$\left|\frac{\tilde{P}(jw)}{P(jw)} - 1\right| \leq W(jw) \quad \forall w. \tag{4.32}$$

This perturbation, or uncertainty profile represents the expected multiplicative disturbance for a given magnitude of current change, and gives the range for determining a set of possible perturbed models. The MPC controller needs to be stable for all these perturbed models. In order to determine these uncertainty profiles, the non linear model is simulated over a variety of desired current changes and the LPV model at each current measurement is compared to the LPV model calculated using the current at the next time step. The difference between these models is used to calculate the perturbation (W) between them (using (4.32)). This procedure is repeated over a variety of operating conditions and produces a perturbation for each current magnitude change. Since we are simulating each current magnitude change over a large number of operating points, the maximum pertubation at a given frequency is used, thus ensuring our model is stable for a worst case condition. The uncertainty profile is then found for a pre-determined set of expected current change magnitudes. We would expect that the uncertainty will be very high for large changes in current, and smaller for decreasing magnitude changes. The current trajectories used to calculate the expected perturbations are shown for current changes of 0.0, 0.05, 0.1, 0.15, 0.2, 0.5, and 1.0 amperes/second in Figure 4.4. For each of the current change magnitudes, an expected perturbation is fitted using (4.32). This is done using the maximum difference at each frequency for all the available data points that incorporate the expected current change magnitude. The perturbation profiles for each magnitude change are shown in Figure 4.5 and Figure 4.6. These plots show the maximum gain for each input and frequency for a given rate of current change. The comparison is made using the difference between two models (the nominal P and perturbed model $\tilde{P}$), so a higher gain represents a larger perturbation. It is clear that as the demand current is allowed to change at larger rates, the model differences increase quickly in magnitude.

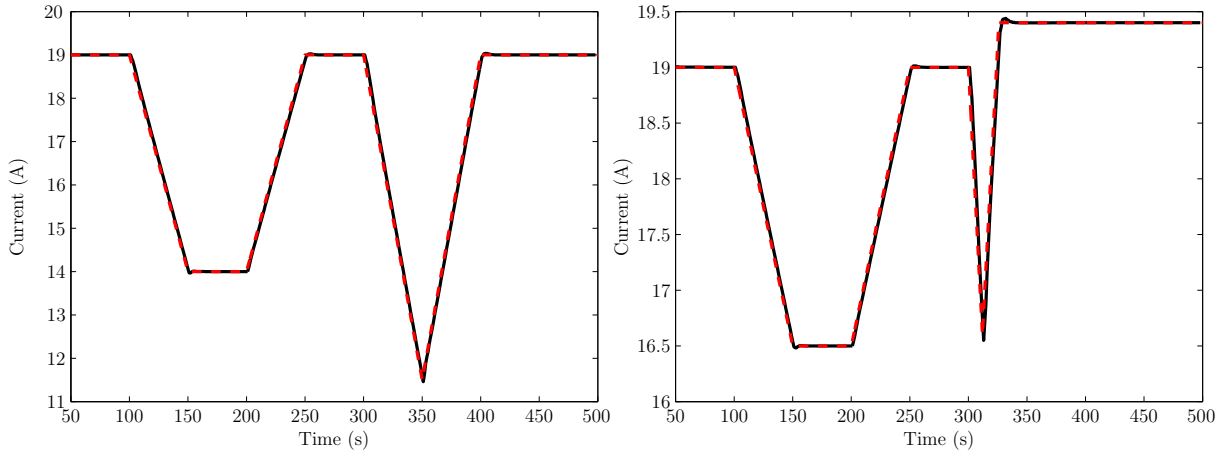

(a) Magnitude changes of 0.1 and 0.15 $\frac{A}{s}$.

(b) Magnitude changes of 0.05 and 0.2 $\frac{A}{s}$.

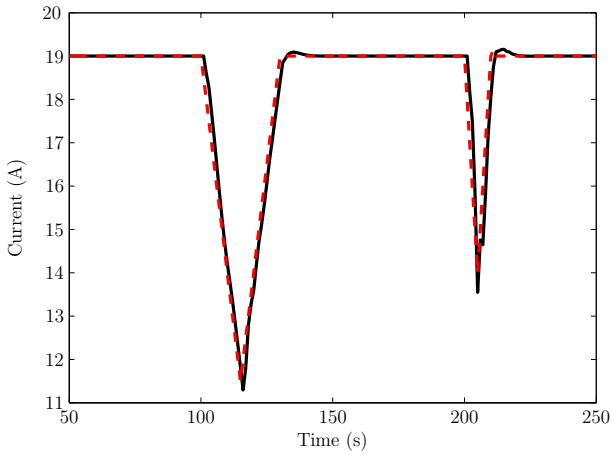

(c) Magnitude changes of 0.5 and 1.0 $\frac{A}{s}$.

Figure 4.4: Plot of the system current (black and solid) and the desired current (red and dashed) for various magnitude changes.

Using the expected noise profile, and the transfer function of the controller, a stability test is then carried out to determine if the amount the desired current is changing will result in instability. Define a sensitivity funciton:

$$T = \frac{PC}{1 + PC}. \tag{4.33}$$

Then using the multiplicative uncertainty model in (4.31), the controller is stable for the perturbation if:

$$\|WT\|_\infty < 1. \tag{4.34}$$

For a proof of this result refer to Doyle et al. [68]. Thus at each timestep, if the controller

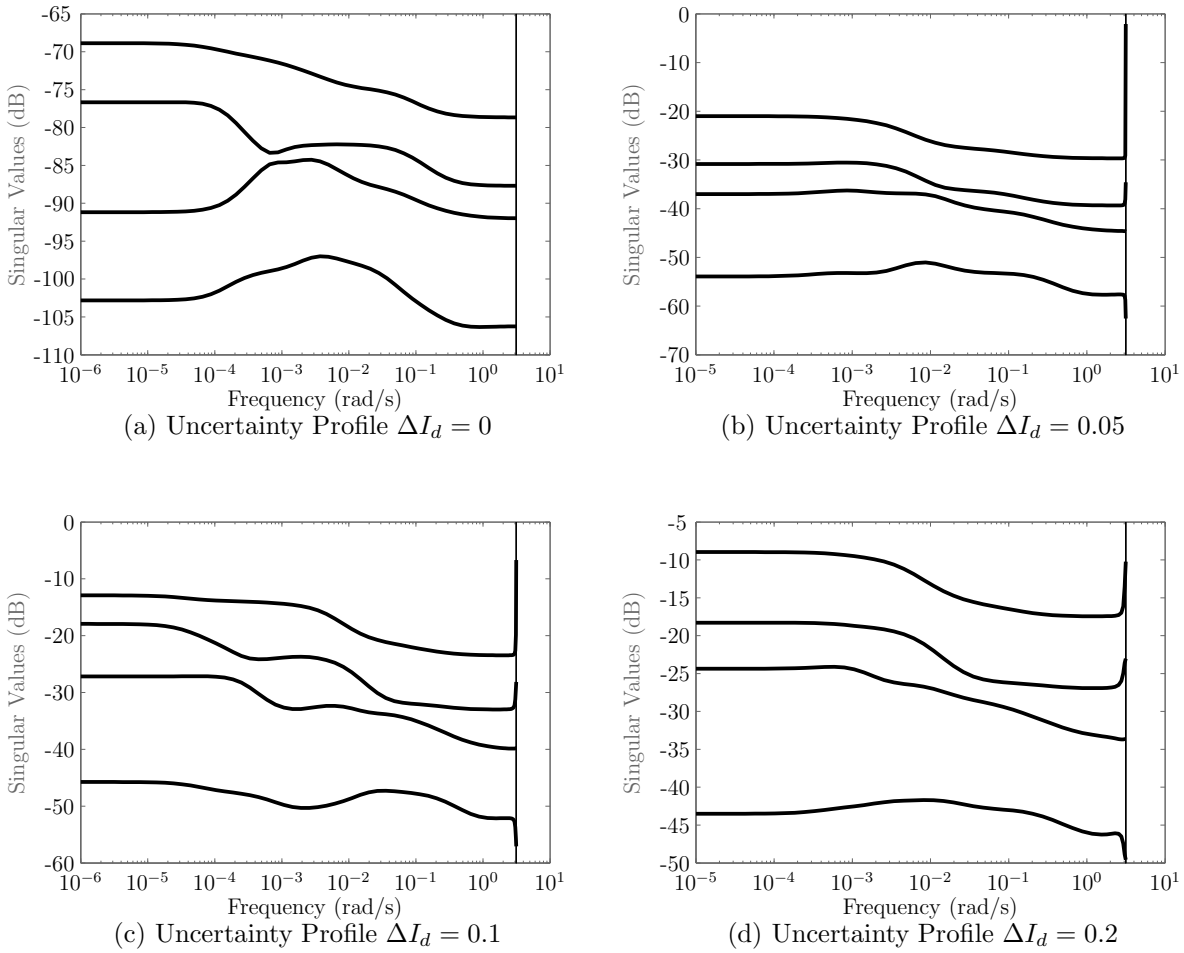

(a) Uncertainty Profile $\Delta I_d = 0$

(b) Uncertainty Profile $\Delta I_d = 0.05$

(c) Uncertainty Profile $\Delta I_d = 0.1$

(d) Uncertainty Profile $\Delta I_d = 0.2$

Figure 4.5: Magnitude plots of the uncertainty profiles for various current demand changes

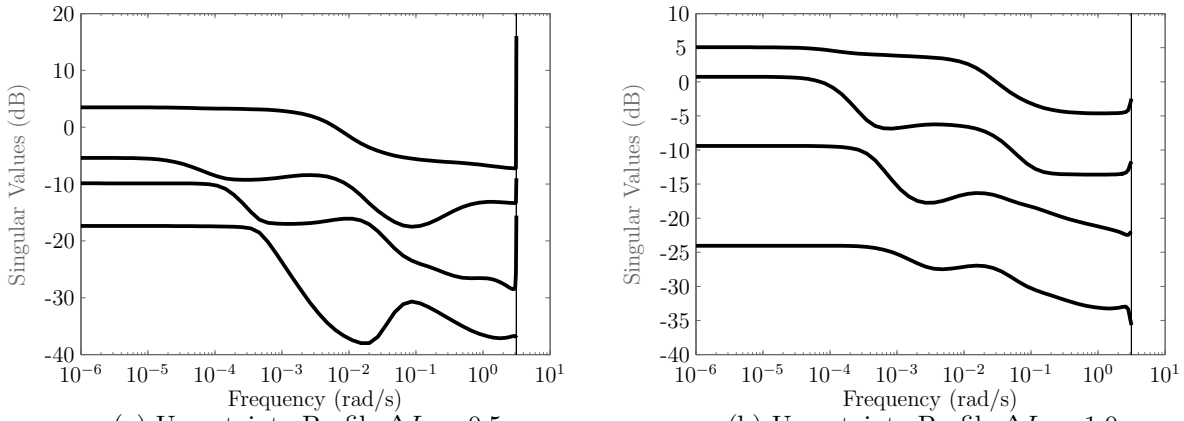

(a) Uncertainty Profile $\Delta I_d = 0.5$ (b) Uncertainty Profile $\Delta I_d = 1.0$

Figure 4.6: Magnitude plots of the uncertainty profiles for various current demand changes

transfer function and an uncertainty model is available, it can be determined if the given controller is stable for the uncertainty model (if (4.34) holds). However, the MPC controller is not available in a closed form solution, only as an optimization problem. As the cost function is similar to an LQR controller (4.35), a substitute LQR controller transfer function is therefore used in (4.33).

$$\begin{aligned} J = \underset{u}{\text{minimize}} \quad & x_N' Q_f x_N + \sum_{i=0}^{N-1} x_i^T Q x_i + u_i^T R u_i \\ \text{subject to} \quad & x[i+1] = Ax[i] + Bu[i] \end{aligned} \tag{4.35}$$

The LQR controller is calculated using identity weights and the current LPV model. The use of an LQR controller in the sensitivity function (4.33) is an approximation. The LQR controller does not enforce system constraints so it will surely produce a different calculated input. Ideally the MPC controller could be determined in a closed form. However, since the model and objective changes every time step, as well as over the horizon window, this closed form is not available. Using the pre-calculated uncertainty model (Figure 4.5, Figure 4.6) corresponding to the current magnitude change and the estimated LQR controller an approximate measure of stability can be found. Due to the LPV dynamics and the use of an MPC controller, this measure is not a guarantee of stability. It does, however, provide a

useful measure of how close a similar controller is to being stable for all frequencies of inputs. If the desired load change is unstable, a smaller change can be incremented until the actual desired current is reached. Thus implementing a stability based rate limiter on the allowed current change. The algorithm for the rate limiter is summarized below:

```
 calculate P
 calculate T using LQR controller for P
 while (fail = 1)
      determine expected perturbation W
      robust = norm(WT,inf);
      if robust > 1
         reduce desired current by factor of 2
         calculate P
         calculate T using LQR controller for P
      else
         fail = 0
end while
```

At the conclusion of the algorithm the desired current magnitude is reduced until the LQR controller can stabilize all models within the expected perturbation.

CHAPTER 5

RESULTS

Results for this work are analyzed in four sections. The response and dynamics of the non-linear model are analyzed to determine what impact specific components have on the time response of the system and how they limit load changes. It is determined that the blowers are critical to operating within constraints. The estimation of the reformer inlet fuel composition is presented. The identification and reduction to a LPV model structure is also analyzed. Finally the ability of a MPC algorithm to drive the current to a desired value while not violating constraints is tested, as well as the sensitivity of the controller to changes in the scheduling parameter.

5.1 Open loop Response

Analysis of the system model provides excellent motivation for the development of an MPC controller to ensure stable and safe operation of the system. For example, with both the fuel reformer and stack air flows supplied via blowers, the dynamic response of the blowers is critical to the ability of the reformer and stack to respond to demand changes. For large increases in current demand, the supply of fuel to the reformer can be increased much more quickly than the air since the blowers are much slower than whatever valve is used to regulate fuel flow. This dynamic mismatch will result in compositions that temporarily have very low ratios of $\frac{O_2}{CH_4}$, and can lead to carbon deposition in the stack. An increased current load can also produce very undesirable fuel utilization because the air blower time constant is slower than that of the reformer fuel supply. This effect is shown in Figure 5.1 for step changes in between different operating conditions. The simulation in Figure 5.1 involves step changes across a variety of operating conditions, from low current (approximately five amps) with fuel utilization varying from 45% to 76% and reformer inlet $\frac{O_2}{CH_4}$ ratios from 1.13 to 1.52. Thus for following load changes the speed at which the blowers can achieve

the proper air/fuel mass balance is the limiting system dynamic. Temperature dynamics are much slower and require slow manipulations of fuel and airflow to stay within limits. The exception to this rule is the burner temperature. Although not considered as a constraint, if the amount of hydrogen to be combusted is very high, it is possible to quickly exceed the operating temperature of the burner. An implemented controller must be able to choose between the various mass flow, $\frac{O_2}{CH_4}$ ratio combinations in order to produce the desired current without violating temperature, utilization, and coking constraints.

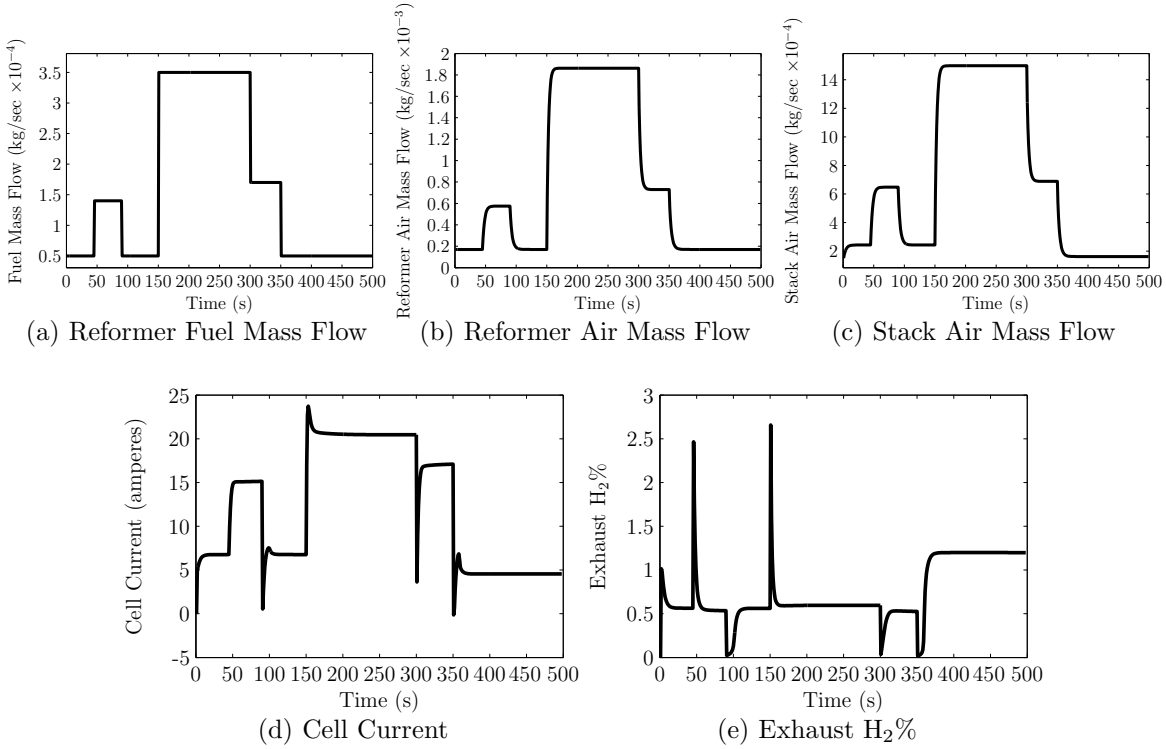

(a) Reformer Fuel Mass Flow (b) Reformer Air Mass Flow (c) Stack Air Mass Flow

(d) Cell Current (e) Exhaust H_2%

Figure 5.1: Open loop dynamic response.

5.2 Fuel Composition Estimation

Utilizing an EKF allows for calculation of the unknown biogas composition using only the reactor temperature as a measurement. Results are presented using the model, and the experimental setup described in Chapter 3. The model used within the EKF is a non-linear DAE system with uncertainty in the composition of the reformer fuel. The fuel

composition uncertainty is quantified as a bias (a difference from an assumed percentage of methane). The fuel composition is assumed to consist only of methane and CO_2, so any increase in methane results in a corresponding decrease of CO_2. The EKF combines the temperature measurement of the real system with the calculated measurement of the model to estimate this composition uncertainty. Within the experimental system, the temperature measurement consists of a type K thermocouple, which has an accuracy representative of what would be used in a non-experimental system. The inlet gas flows are controlled by mass flow controllers (MFCs), which would most likely be blowers in a production system. The MFCs are much faster and more precise than a blower, but since they are not used as measurements, but instead to create the unknown gas composition, their use does not affect the observability of the inlet bias. Using the model, a simulation of the CPOX reactor

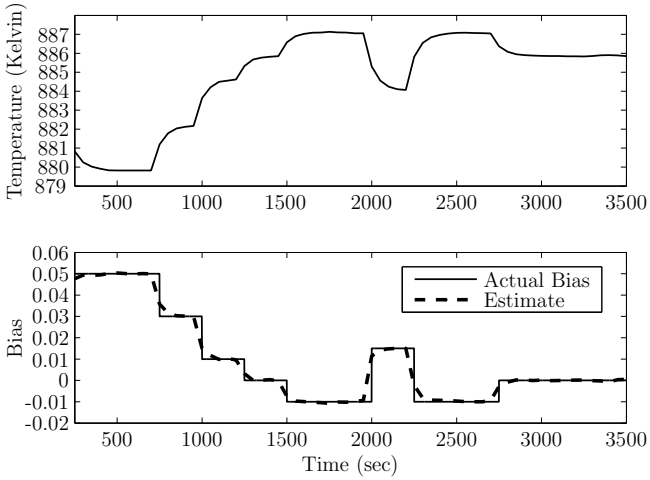

Figure 5.2: Reactor Temperature and Bias, Simulated Data

with several step changes in fuel composition was performed, with $\mu = .96$, and constant air and fuel mass flows. The resulting temperature of the CPOX reactor and the fuel variation (represented by the bias) are shown in Figure 5.2. This temperature, along with the nominal inputs were given to the estimator, and the estimate is also shown Figure 5.2. The results show that good convergence to the correct inlet composition bias is achieved. The ability of the estimator to converge to the correct bias estimate depends heavily on the sensitivity

of temperature to perturbations in the biogas compositions. In operating regions where the amount of methane compared to CO_2 has no impact on the temperature, the uncertainty of the estimated bias is high. Such an unobservable region would include start up or cool down, where often a heated non-reactive inlet gas is used to bring the temperature of the reactor to a minimum value. Additionally, since the bias represents a perturbation to an assumed composition, for extremely high $\frac{O_2}{CH_4}$ ratios the uncertainty of the bias estimate will increase as the amount of methane is extremely low. Under such a condition, an increase in methane content by a few percent has no effect on the temperature. Neither of these cases represent operational conditions of an actual plant, however. It was observed that for $\frac{O_2}{CH_4}$ ratios from 0.5 and higher the bias estimate converges. When the bias is positive, there is more CH_4 than anticipated, in effect reducing the $\frac{O_2}{CH_4}$ ratio, and thus dropping the temperature. The opposite is observed for reduced CH_4, as the $\frac{O_2}{CH_4}$ ratio increases and the reactor temperature increases correspondingly.

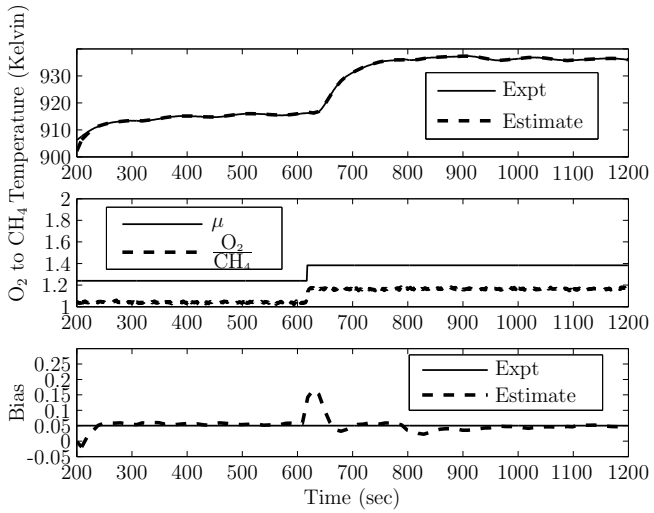

Figure 5.3: Estimated Temperature, single μ, and Bias, Experimental Data

The estimator has also been tested using the experimental reactor. These tests provide a much more realistic result than the model based data, since noise is now present in both the model and the measurement. The experimental conditions were 2 SLPM total flow of air and fuel with a step change from $\frac{O_2}{CH_4}$ ratio of 1.03 to 1.25. The results are shown in Figure 5.3.

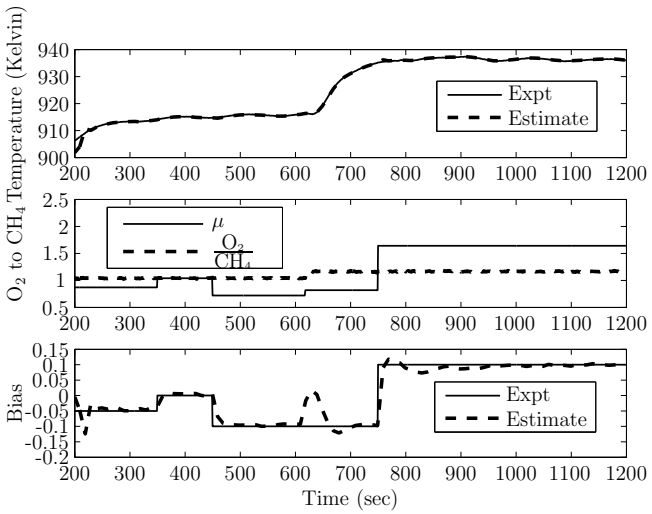

Figure 5.4: Estimated Temperature, multiple μ, and Bias, Experimental Data

This step change results in a temperature increase for the reactor. The initial EKF estimate of the inlet composition is 65% methane while the actual gas contains 70% methane. After oscillating for several time steps, the filter converges on the correct bias within 1.0%. The variance of the bias estimate as determined by corresponding element of P_k remains constant for both operating conditions. In order to represent a more rapidly changing biogas stream, Figure 5.4 shows the same 2 SLPM total flow and $\frac{O_2}{CH_4}$ ratio step for multiple μ conditions. For Figure 5.4 the assumed fuel composition (μ) is varied. The bias is then measured against differing base conditions. For a varying μ the estimate converges to the actual composition within 1.0% CH_4, for both operating conditions. The only large transient bias estimate errors occur due to an erroneous initial condition (when the filter initially estimates the bias) or coincide with the step change in the $\frac{O_2}{CH_4}$ ratio at approximately 650 seconds. The large error at 650 seconds (during the step change) is the result of model mismatch. Specifically, the model predicts a faster temperature response than is observed in the experimental system. This time response discrepancy is clearly shown in Figure 5.5, with the model predicted temperature rise occurring several seconds before the temperature change is measured. The step change in temperature shown in Figure 5.5 is for the same $\frac{O_2}{CH_4}$ ratio change as Figure 5.3 and Figure 5.4. The temperature response of the model is compared to the temperature

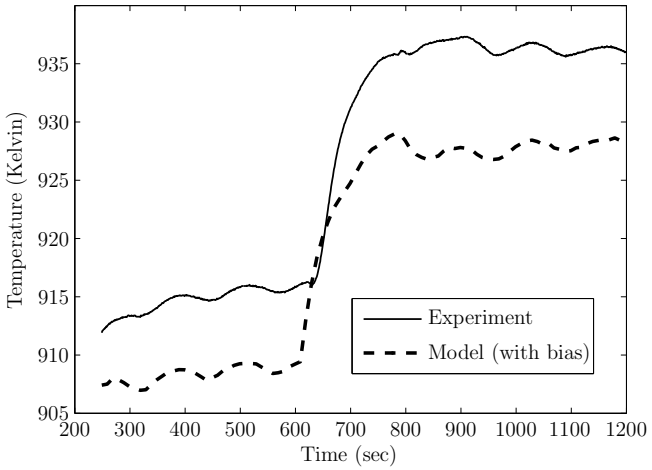

Figure 5.5: Reactor Temperatures for Experiment and Model (without Kalman filter correction) with Bias

response of the experiment, showing the effect of the bias on the temperature, as well as the difference in dynamic response. The effect of the bias is shown as the model result is plotted without the Kalman filter correction. Without this correction, the bias causes an offset between the model temperature and the measurement. The model transient mismatch is most likely due to errors in the thermal mass constants of the control volumes. The error is unlikely to be a problem in an actual system since the biogas composition changes much more slowly than the rapid step changes simulated in this experiment.

5.3 System Reduction

This section will discuss how accurately the identified LPV model can match the nonlinear model. Using the perturbation experiment discussed in Section 4.1, a seven state, five output, four input LPV model, scheduled using the current and MEA temperature was identified. Using a seperate validation input (shown in Figure 5.6) the fit between the model output and simulation is shown in Figure 5.7. Ideally the identified linear model would perfectly produce the outputs measured when given the known input sequence. The results in Figure 5.7 are for a one step ahead predictor. That is, the state is assumed to be fully measured at each time step, and the identified model is used to predict the impact of the

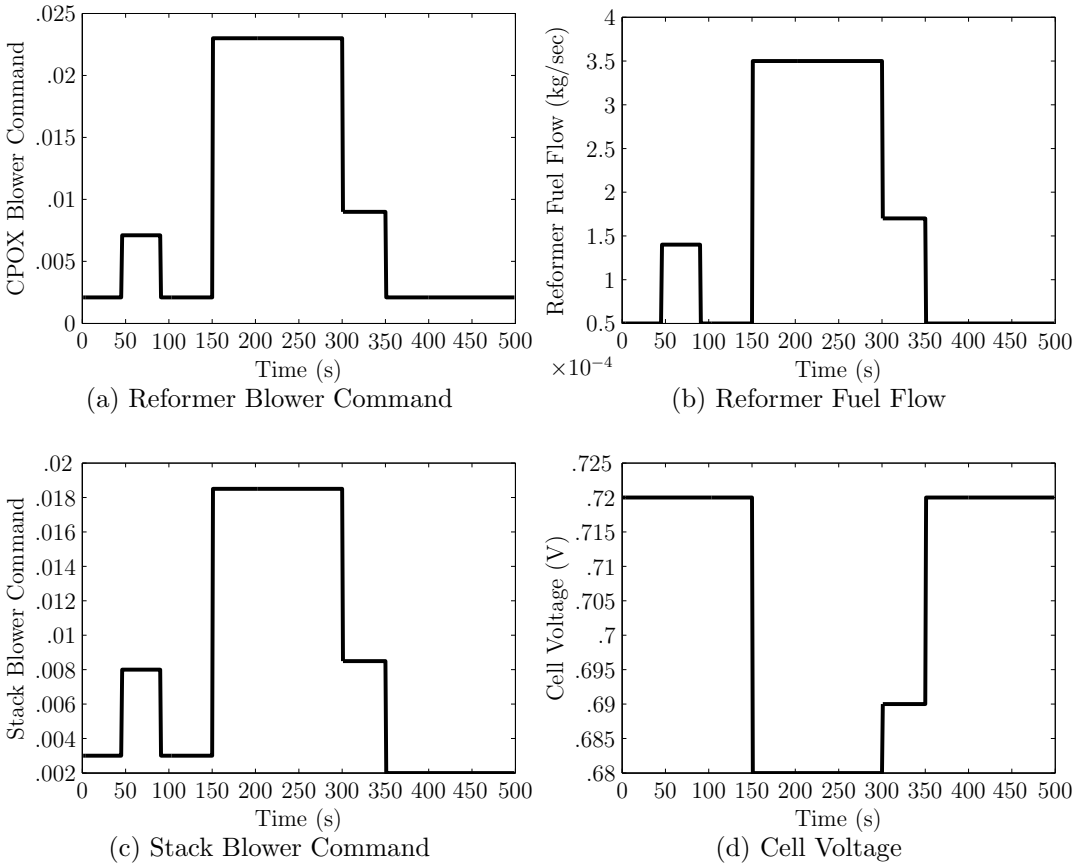

(a) Reformer Blower Command

(b) Reformer Fuel Flow

(c) Stack Blower Command

(d) Cell Voltage

Figure 5.6: System Identification Inputs

applied inputs to the state and the outputs at the next timestep. These plots thus express the accuracy of the LPV model when used in a system where all outputs are measurable. In this case the LPV model is only required to estimate one timestep ahead, given the inputs to be applied and the current system state. This is a very favorable condition for the model

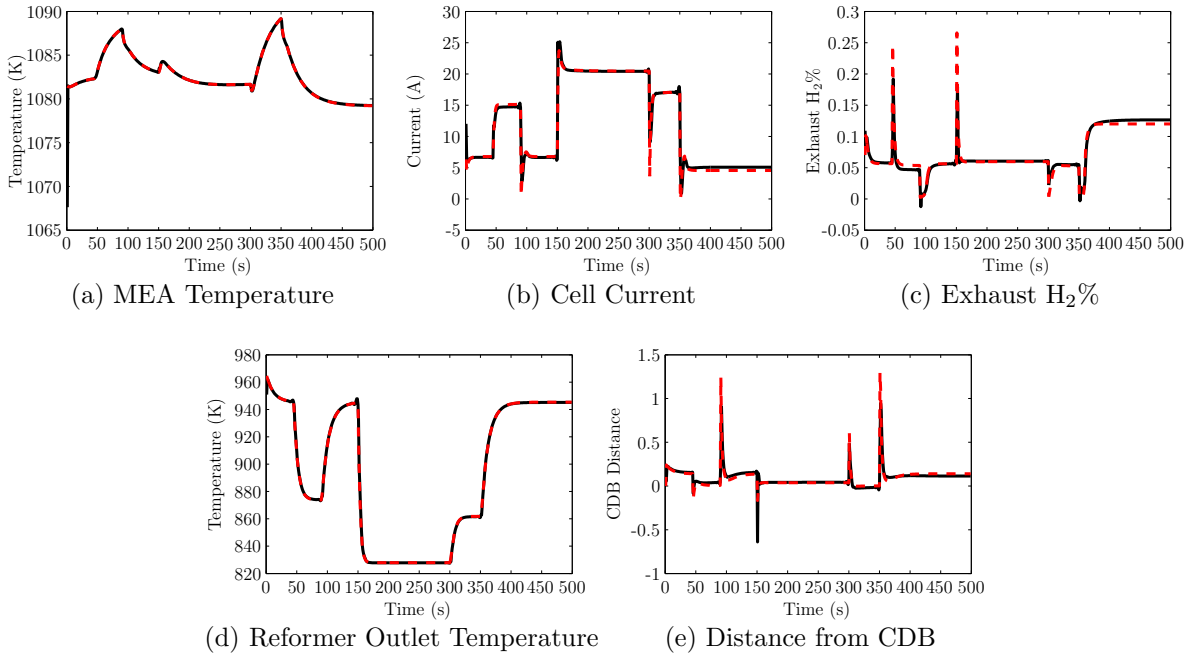

(a) MEA Temperature (b) Cell Current (c) Exhaust H_2%

(d) Reformer Outlet Temperature (e) Distance from CDB

Figure 5.7: System Identification Results, identified model is solid and black, nonlinear model is red and dashed.

comparison, as evidenced by the very close match between predicted and observed values between the linear and nonlinear model. On the extreme other end is a straightforward simulation with the predicted inputs applied. In this case, only the measurements at time 0 are used (to estimate an initial state). Once the initial state is estimated, no further measurements are used. The only information used is the known input sequence. The results of this simulation are shown in Figure 5.8, and are markedly worse than the one step predictor. The system shows a drift from the actual values, as would be expected with no measurement to correct the model. However, for the SOFC system we are interested in controlling, three of the outputs are measurable. A more useful representation of the accuracy of the LPV model is to combine the simulation with a Kalman filter, which makes use of

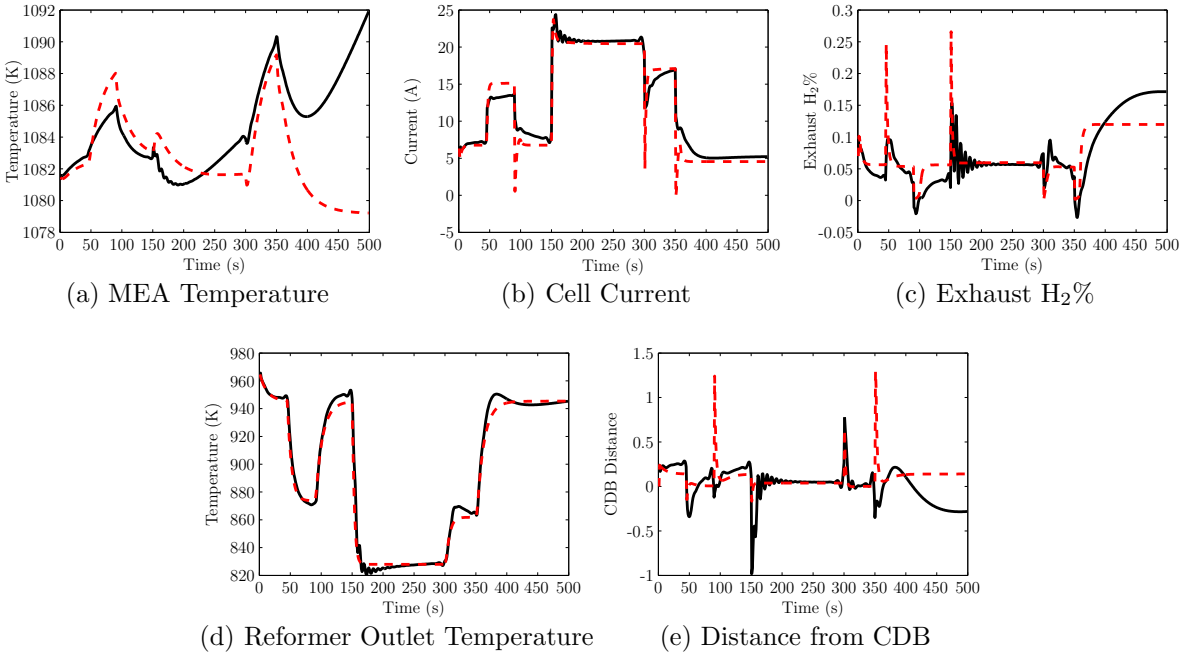

(a) MEA Temperature (b) Cell Current (c) Exhaust H_2%

(d) Reformer Outlet Temperature (e) Distance from CDB

Figure 5.8: System Identification Results without measurements, identified model is solid and black, nonlinear model is red and dashed.

the model and measurements to estimate the unknown outputs. The LPV model simulated with a Kalman filter is shown in Figure 5.9. This combination is the most representative of the conditions the controller will face in an actual system, with temperature measurements available, but composition measurements requiring estimation. Only the two estimated outputs are plotted, as the measurements are highly trusted and the model is used only to calculate the unknown outputs. The values of the measured outputs are weighted such that the measurement is trusted much more than the model prediction. The two unmeasureable outputs are much more challenging to estimate using the LPV model. From Figure 5.9 it can be seen that for some operating conditions the H_2 exhaust concentration has errors up to 1%. This magnitude of error requires the controller to be tuned to operate at an artificially high exhaust concentration in order to not violate constraints. The same is true for the carbon deposition distance which has errors as high as 0.05. The magnitude of error in the CDB distance calculation is very high considering the range of operation is often within 0 to 0.2. Thus the controller must be tuned to force the system to operate above a 0.0 CDB distance

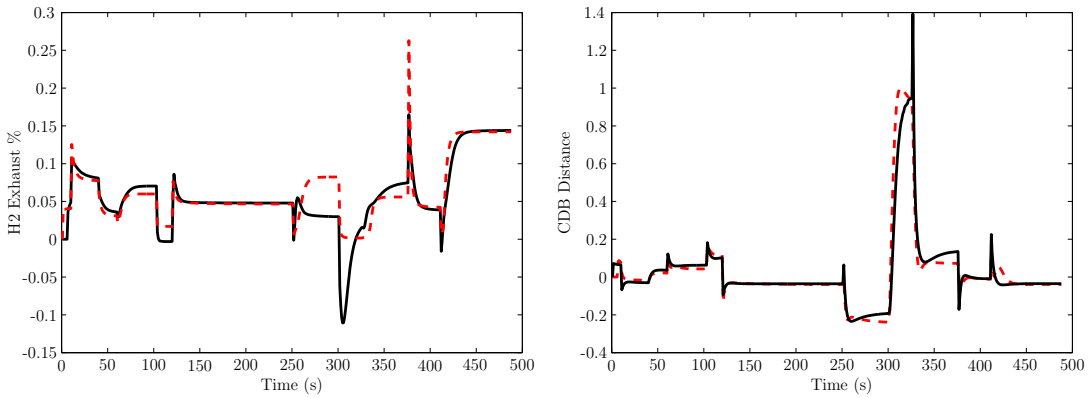

(a) H_2 Exhaust % (b) CDB Distance

Figure 5.9: LPV model results with Kalman filter. The LPV and Kalman estimate is black and solid, while the nonlinear model is dashed and red.

to accomodate this error.

The performance of the estimated model is measured using a VAF value, calculated as:

$$VAF_{y_i} = \max\{1 - \frac{var(y_i - \hat{y}_i)}{var(y_i)}, 0\}(100). \tag{5.1}$$

Where $i = \{1..l\}$, thus there is a VAF score for every output. For the desired, 4 input, 5 output system, identification of a system with three blended linear models of state size 7 resulted in an acceptable VAF fit for a validation data set. Using the current and MEA temperature as scheduling variables gives VAF scores (for the one step ahead predictor) of 97.8927 for the MEA temperature, 99.5377 for the current, and 99.9619 for the reformer temperature. The remaining outputs have VAF scores of 84.2987 for the exhaust H_2% and 93.8894 for the CDB distance. These values are for the same test run used in the identification experiment. When testing the identified model on data sets other than that used for identification (but still within the same operating range) the VAF scores dropped for the two unscheduled variables to approximately 80 to 90 for the exhaust H_2% and 60 to 90 for the CDB distance. Both temperatures are identified very well, with the LPV model predicting the nonlinear model within 0.5 K. The current also shows excellent identification with errors remaining within one ampere. The range of operation for the identification experiment is also quite challenging, consisting of a large number of operating points for the

SOFC system.

The choice of measurements used to build the scheduling variable is also a very important design consideration. Limiting the scheduling variable to measured outputs gives three variables as possibilities: the current, the MEA temperature, and the reformate temperature. The scheduling variable has rows equal to the number of models in the identification set ($\mu \in \mathbb{R}^{m \times L}$). Thus, if only one model is in the identification set, or $m = 1$, the scheduling variable is an identity vector. If the number of models to be combined is 2, or $m = 2$, the identity vector is used for the first row, and one of the available measurements is used for the second row. As additional models are added to the identification set (increasing m), the scheduling variable must affinely combine them using additional rows, as in Eq. 4.1. Thus additional measurements must be included, calulated from the existing measurement(s). Orthonormality of the vectors used as rows within the scheduling variable is not required, but greatly improves the conditioning of the result. All possible combinations of the measured variables were tested to determine what the most effective scheduling sequence is for the system. Results of a parametric analysis for a variety of model state sizes (n) and identification window (p) are included in Figure 5.10. For each included measurement within the scheduling variable, the number of states and prediction window was varied. Scheduling using the current alone Figure 5.10(a) achieved a combined VAF ($\frac{\|\{VAF_1,VAF_2,VAF_3,VAF_4,VAF_5\}\|_1}{500}$) of 91.23. Using the reformate temperature alone as a scheduling variable, resulted in a combined VAF of 88.38 (Figure 5.10(b)). Utilizing only the MEA temperature as a scheduling variable resulted in a combined VAF of 86.27 (Figure 5.10(c)). For all three cases the maximum score was achieved for seven states and a prediction window of $p = 2$.

Expanding to include multiple measurements as rows of the scheduling variable tends to slightly decrease the VAF scores for the identification experiment (Figure 5.11). Utilizing current and the MEA temperature results in a combined VAF of 86.25, while using the current and reformate temperature gives a combined VAF of 86.69 (Figure 5.11(b)). Utilizing just the two temperatures gives a combined VAF of 86.14. While scores for the

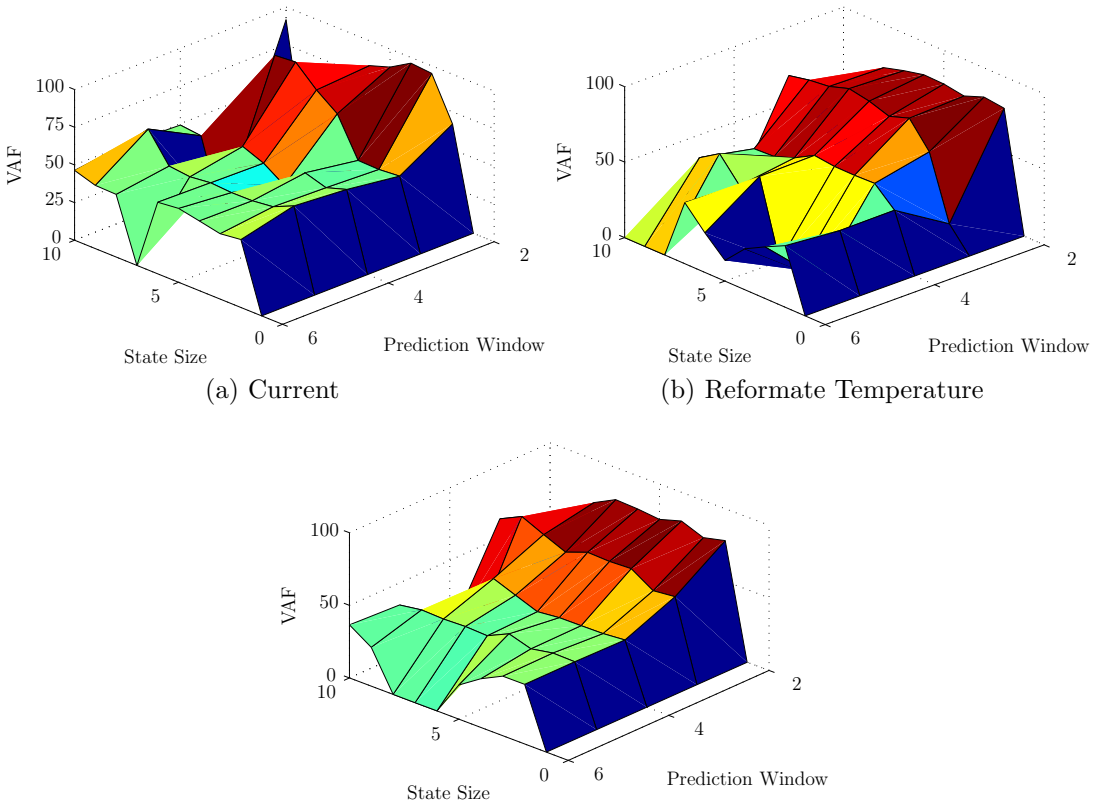

(a) Current

(b) Reformate Temperature

(c) MEA Temperature

Figure 5.10: Combined VAF for all five outputs, scheduling using only a single variable.

combined measurement scheduling variable are slightly lower, controllers designed using multiple measurements exhibited less oscillation when changing operating points, allowing for faster current changes (this oscillation is discussed later in this chapter). This result is due to the rapidly changing current being mitigated by the much slower changing temperature variable, reducing the impact of very fast current changes on the model dynamics. The VAF scores were also very similar for scheduling using the current and MEA temperature and scheduling using the current and the reformate temperature. However, controllers designed using the MEA temperature performed better. For these reasons the model used for the results presented in this work is a seven state model ($n = 7$), with a prediction window of two ($p = 2$), scheduled using the current and the MEA temperature ($m = 3$).

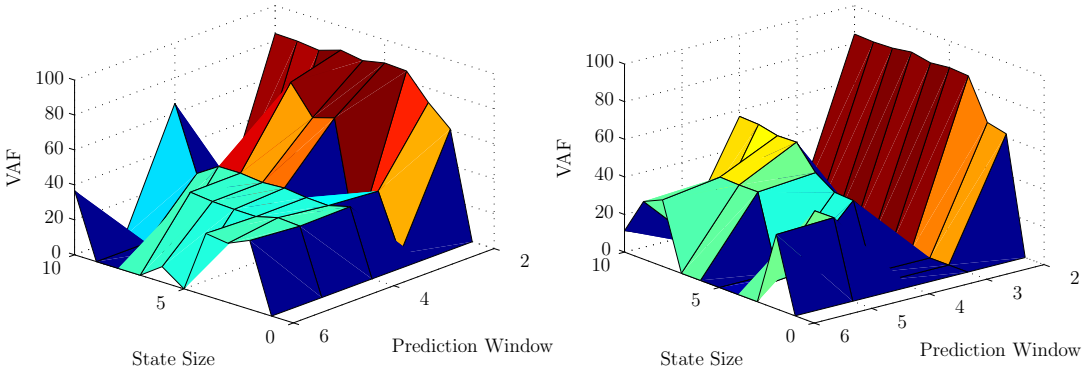

(a) Current and MEA Temperature

(b) Current and Reformate Temperature

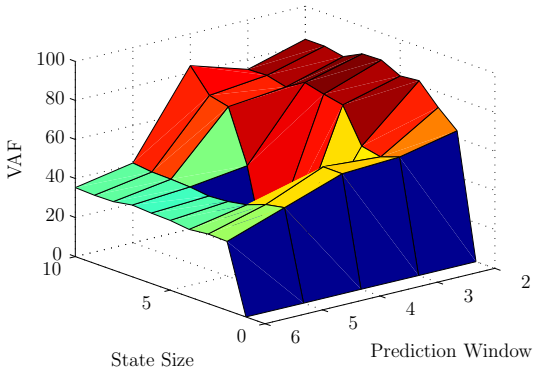

(c) MEA and Reformate Temperature

Figure 5.11: Combined VAF for all five outputs, scheduling using a combination of two outputs.

5.4 Model Predictive Control

In order to test the ability of the the MPC controller to follow loads without violating constraints the controller is tested on the nonlinear model. The controller was tested over a variety of output conditions and shows generally good load following ability over the operating current range (Figure 5.12). In addition the controller is able to stabilize the current within the desired range. Additional results are shown for a current demand step

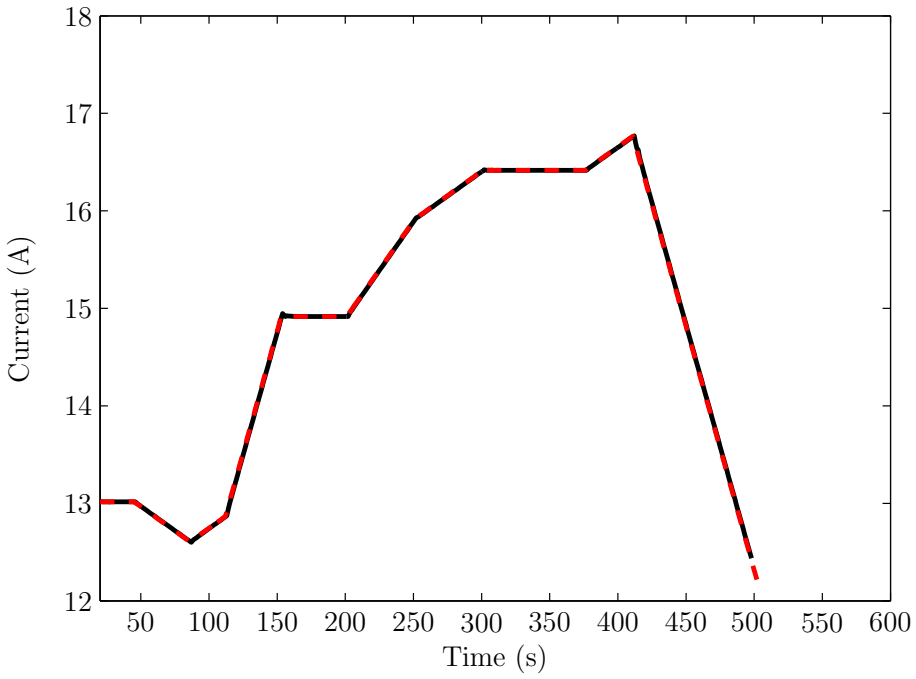

Figure 5.12: Controller results for a load following trajectory. Desired current is dashed and red, system response is solid and black.

both down and up of 1.0 amperes per second and 0.1 amperes per second in Figure 5.13. In both cases the controller is able to closely meet the current demand, however the fast current step causes a much larger oscillation (Figure 5.13(a)) than for the slow demand change (Figure 5.13(d)). The output constraints are also violated for the large demand change, shown in Figure 5.13(b) and Figure 5.13(c). The controller is thus capable of load following while not violating any of the system constraints, for a limited rate of current change.

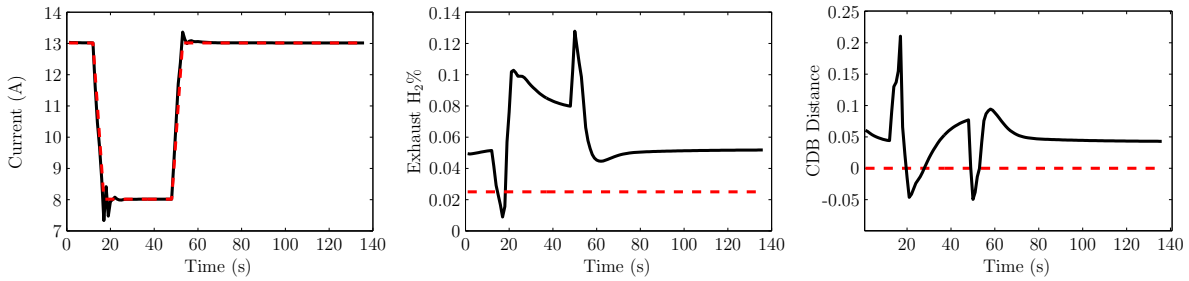

(a) Current Response Fast Step (b) Exhaust H_2% Fast Step (c) CDB Distance Fast Step

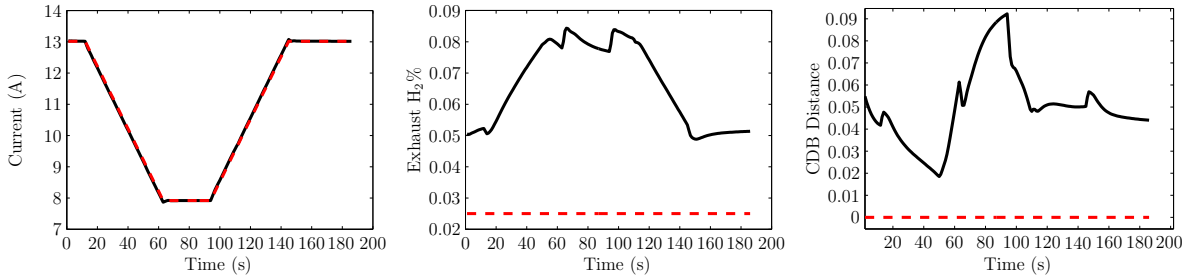

(d) Current Response Slow Step (e) Exhaust H_2% Slow Step (f) CDB Distance Slow Step

Figure 5.13: Controller results for a fast and slow current demand change. Desired current is dashed and red, as are hard constraints. System response is solid and black.

The reason that the current trajectory rate change must be limited is that the MPC controller operates over a prediction horizon. The model used for the optimization is generated from the LPV model and fixed over this prediction horizon. A fixed linear model greatly decreases the complexity of the resulting optimization problem, but introduces modeling error. The effects of this modeling error on the calculated inputs is shown in Figure 5.14. For the fast step, the MPC calculated inputs overshoot, as the model at the current output has different dynamics than the model at the the desired current output.

To visualize the model discrepencies faced by the controller, we utilize a k-step predictor where k is equal to the MPC horizon. The results of a $k = 7$ step predictor are shown in Figure 5.15. The controller model faces large transient errors in H_2 exhaust concentration and CDB distance over the horizon, as shown in Figure 5.15(c) and Figure 5.15(e). These results are for the same input sequence as that used in Figure 5.7 and Figure 5.9. The MPC controller thus has a discrepency between the predicted dynamics, which are used for the optimization, and the dynamics which are used for the optimization at each successive time

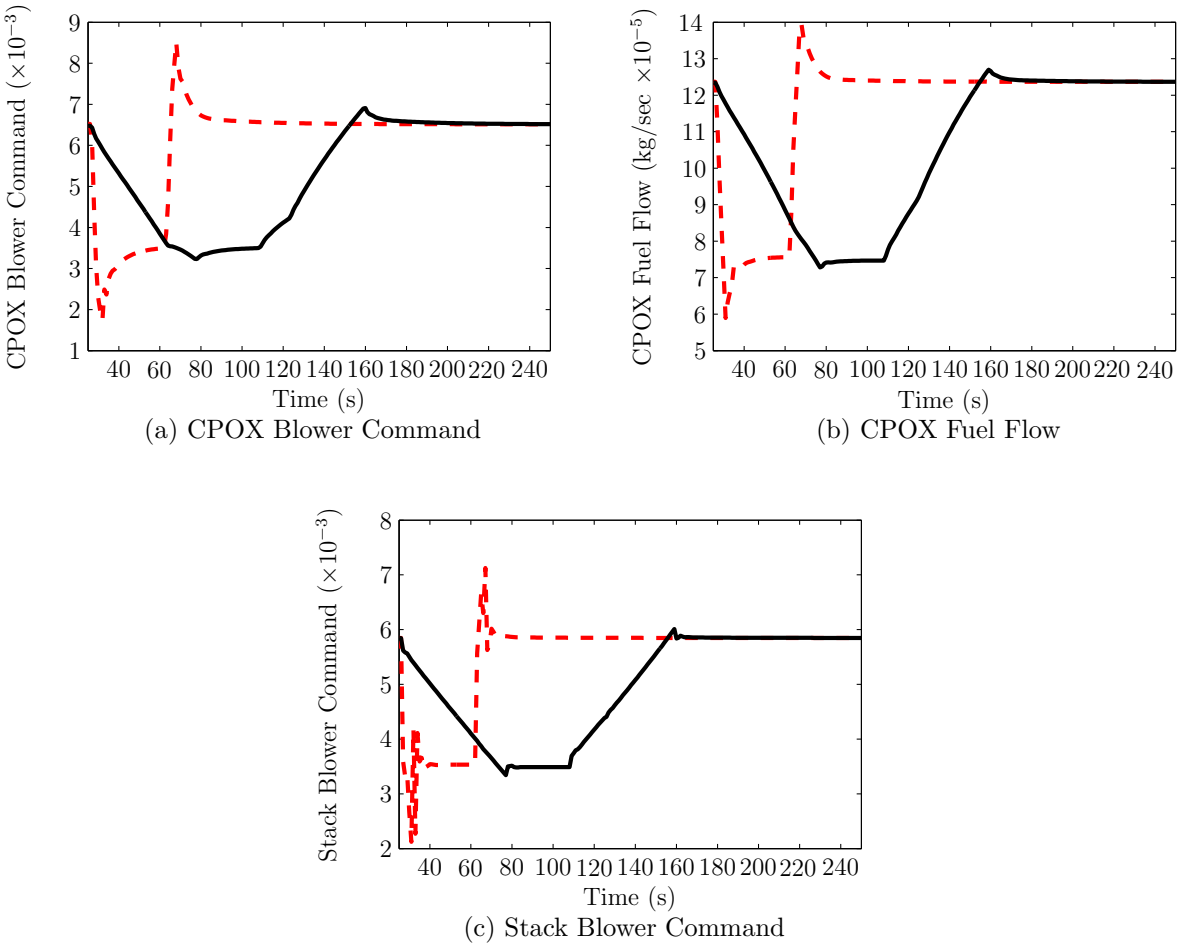

(a) CPOX Blower Command

(b) CPOX Fuel Flow

(c) Stack Blower Command

Figure 5.14: MPC calculated inputs for the fast (red and dashed) and slow (solid and black) steps.

step. If the current demanded is allowed to undergo large step changes, the dynamics at the next time-step may be different than predicted, and thus the calculated inputs will show a large error. The controller will eventually converge to a new model, but oscillation will occur around the new set-points. The magnitude and length of the oscillation is dependent on how far away the current MPC model is and thus how inaccurate the effects of the calculated outputs. Violation of hard constraints can occur during these changes as well for the same reasons. The MPC still calculates inputs that do not cause output violations, but the model it uses to do so is inaccurate over the horizon. In addition this mismatch is not equal at all operating points. For some regions, the LPV model is very close, thus allowing fast current

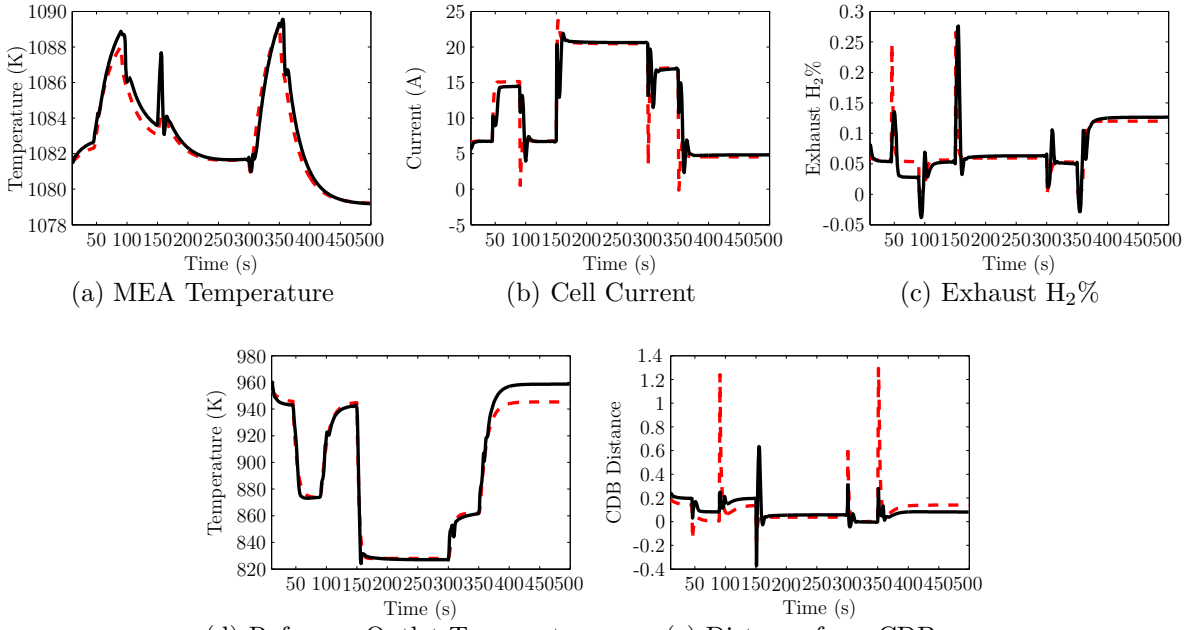

(a) MEA Temperature (b) Cell Current (c) Exhaust H_2%

(d) Reformer Outlet Temperature (e) Distance from CDB

Figure 5.15: $k = 7$ step predictor, identified model is solid and black, nonlinear model is red and dashed.

changes, in other regions, the LPV model is inaccurate, requiring a limitation on the allowed magnitude of current change. The effect of this mismatch is prominently displayed in errors between the MPC predicted current (or the current demanded) and the actual system current which is measured.

Implementing some form of LPV MPC should greatly reduce this problem, although with a cost of increasing the complexity of the controller. Alternatively, the rate of change for the scheduling variables can be limited. For this SOFC system, that requires limiting the allowed rate of current demand change. The controller has no difficulty avoiding constraints with a current demand change of 0.1 amps. The use of a battery or capacitor will be required to limit the magnitude of the desired load change to such a value.

5.5 Rate Limited MPC

The sensitivity of the MPC algorithm to modeling error is difficult to measure. The approach used is to limit the allowable rate of current change based off the current operating

state and predicted error magnitude. The results of such a current limiter are shown in Figure 5.16. The initial current demand change is a step from 19 amperes to 13 amperes, such a large step (7 amperes) would result in an unstable controller until the LPV model settles on the new operating condition. Utilizing the rate limiter to ensure that the controller remains stable for the anticipated range of uncertainty models slows down the load following response, but avoids over and under shoot, thus eventually meeting the desired load change and not violating constraints. The maximum rate of current change allowed by the system

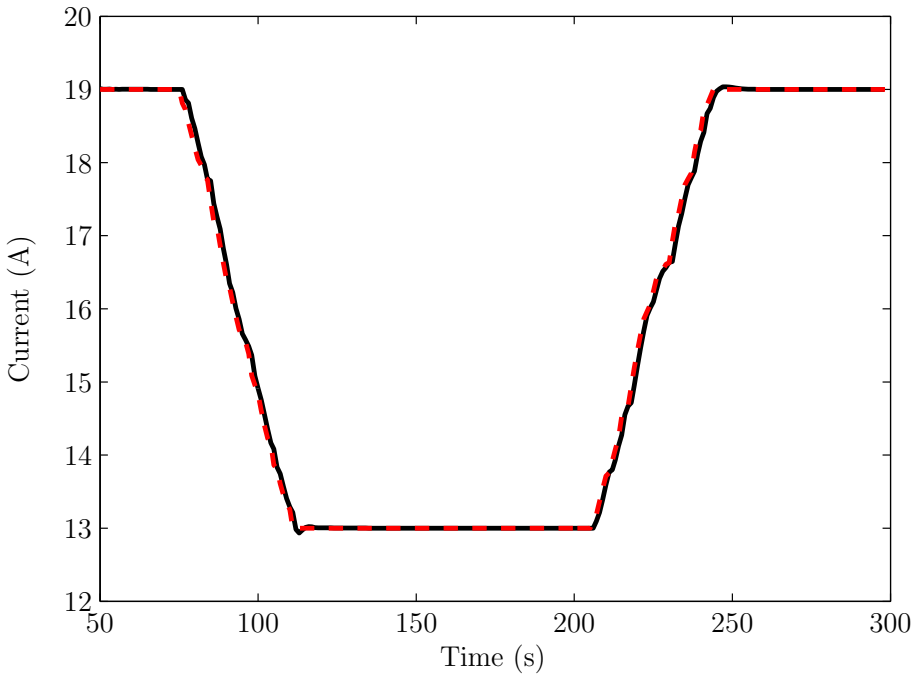

Figure 5.16: Controller results with a rate limited current, black is the controlled system and dashed red is the limited current change.

is approximately 0.15 amperes/second. The allowed rate is not constant, and depends on the difference between the current system dynamics and the dynamics at the desired operating condition. Although the stability based rate limiter does not provide a guarantee of constraint enforcement, in practice it ensures the dynamics stay within a bound. Thus it effectively limits the allowed current change to ensure that the MPC controller will be optimizing using reasonably correct dynamics.

CHAPTER 6
CONCLUSION AND RECOMMENDATIONS

This thesis has presented a high order model of a 1.5 kilowatt SOFC system, composed of a tubular stack, CPOX fuel reformer, blowers, heat exchanger, and tailgas burner. This high order model is then reduced to a LPV model through a system identification process using a global subspace identification technique. Finally MPC is implemented on the identified LPV model and its performance is analyzed with respect to load following. Although this thesis has met the stated goals, several problems remain before such an algorithm could be fully implemented into an existing SOFC system. The following chapter will look at the stated thesis contributions and the problems encountered during modeling, system identification, and control.

6.1 Contributions

The high order modeling of the SOFC system allows for a determination of what effect the BOP components have on the system dynamic response and which components act as bottlenecks to load following. The limiting factor in how fast the system is able to respond to demand changes is the speed of the blowers. Both the electrochemical response of the fuel cell stack and the kinetics in the CPOX reformer are faster than the modeled blowers ability to provide large changes in mass flow. If steam or autothermal reforming is used the reformer dynamics may limit load following response. For small potentially mobile systems, CPOX reforming exhibits an advantageous fast response. The controller was also able to limit the operating temperatures of the reformer by controlling the ratios of air and fuel, while also keeping the temperature of the stack within limits.

The designed fuel reformer estimator is also capable of determining the ratio of CH_4 and CO_2 in an inlet fuel stream. This estimator requires the measurement of the reformate temperature and the fuel reformer model. For a biogas fuel source this estimator can provide

robustness to changing fuel stocks over time, as real biogas production varies slightly. Any variation in fuel composition causes unpredictability in the power produced as well as the temperature and carbon forming properties of the system.

The load following capability of the MPC controller is also determined. Utilizing a stability based rate limiter allows for current changes of approximately 0.15 amperes/second. This imposition of this dynamic limit is not a fundamental physical constraint but a controller issue. The implementation of an MPC algorithm that incorporates the LPV dynamics into the optimization should greatly alleviate the limitation, and allow for calculation of trajectories that allow for faster current changes without violating constraints.

6.2 Implementation Issues

Implementation problems are analyzed in the three aspects of this thesis, modeling, system identification, and MPC. The specificity of the model limits the applicability of this work to a small subset of SOFC systems.

The modeling of any SOFC system will have to take into account the specific geometries and sizes of all components. Models detailed enough to capture all system constraints are thus very system specific. The potential application of the SOFC system determines what fuel sources will be available as well as what reforming methods are preferred. The inclusion of CHP components is also driven by the system application. Any model that is detailed enough to calculate system constraints is unlikely to be suitable for any other system design. Thus the model created for this thesis is applicable to only small tubular stack designs incorporating CPOX reforming. Even then, model parameters would have to be changed and the model performance verified against a physical system or higher order model. The system identification and control aspects of this thesis, however, are applicable to a very broad range of SOFC systems. The identification algorithm is easily adapted to differing sets of constraints and input/output variables. As long as a sufficiently detailed system model exits (CFD or otherwise), the identification algorithm allows for system reduction and control. However, if a dedicated system model must be created, the expense and time

required for implementing system control increases significantly.

Problems with the system identification stem from both experiment design and numerical issues in determining a scheduling sequence. It is difficult to determine a scheduling sequence that is both adequately exciting, and an available measurement of the system. This difficulty is present for SOFC systems but is an issue for any complex non-linear system where there are no clear dynamic "modes" of the system. Experiment design for LPV system identification is also quite nascent. Very good system identification results can be achieved for any single verification dataset, but if they do not represent the operating conditions, they will result in poor controller performance. Often a model that identifies well, performs poorly in estimating the two non-measured outputs, which causes oscillation in avoiding hard constraints. Experimentation is still critical to finding a system identification experiment that produces a model useable within MPC. The large number of experiments required increases the time and cost to developing a control algorithm.

The instability of the MPC algorithm when faced with large current changes stems from two problems. One is the difficulty in estimating the two outputs that are not measurable (the H_2 exhaust concentration and CDB distance). The other is the lack of support for LPV models within MPC. These two problems also compound each other in the actual system. Errors in the estimation of the actual H_2 exhaust concentration and CDB distance imply the current state estimate is incorrect. Thus not only does the MPC controller face changing dynamics due to the LPV model, but the optimization is starting from an erroneous assumption of what the output values (and the current state) are. This can cause feasibility failures in the optimization if the state estimates are too inaccurate, oscillation also occurs if the controller erroneously calculates a constraint violation.

6.3 Future Work

Topics of future work stem from the implemenation issues presented. Modeling of complete SOFC systems is still an active area of research. Modeling of the SOFC system is done with the goal of creating a low order model. Thus the minimum detail of model is chosen,

such that the variables that influence operating constraints are captured. The creation of this model made many assumptions about the geometry, size, and heat transfer characteristics of the system that will most likely differ from any actual system. The results pertaining to the dynamic performance of the specific model are not valid for systems of different size and reforming methods. The specific geometries required to integrate thermal dynamics into the model limits the applicability of any specific model to the myriad engineering approaches used by SOFC system designers. This lack of standardized models makes comparison of different systems and control algorithms difficult. Increased availability of high order models would be benficial to the control community.

In addition to modeling, further work on experiment design for system identification of LPV models is needed. Specifically, how is the determination of a scheduling function best accomplished. The approach in this thesis was rather ad-hoc. Regardless of the model structure used, some combination of measurable variables must be used to differentiate between model dynamics. Identification algorithms that assume a model structure, then fit a scheduling sequence to match input/output data could be very useful in determining what measurements to utilize.

Finally in the area of MPC, there are few algorithms for incorporating LPV dynamics in efficient ways. This is due to rapid increse in dimensions with the addition of varying model dynamics. The MPC optimization problem no longer determines an optimal trajectory with regard to a cost function over a single linear model, but all possible combinations of allowable linear models. With recent reasearch interest into the identification of LPV models that can efficiently represent non-linearities in actual systems, further research is needed on control methods. Specifically, feasible methods for including the changing LPV dynamics within the MPC optimization are required.

The major results of this thesis are published in three derivative works and one work in progress. The first: "M. J. Kupilik, T. L. Vincent, Estimation of biogas composition in a catalytic reactor via an extended Kalman filter, in: 2011 IEEE International Conference

on Control Applications (CCA)" presents the estimation of the inlet fuel composition. The second: "M. J. Kupilik, T. L. Vincent, Model Predictive Control of Reformate Composition for Use in Solid Oxide Fuel Cells, to appear in: 2012 ASME Dynamic Systems and Control Conference (DSCC)" details the use of the MPC controller to manipulate the reformate composition. The third: 'M. J. Kupilik, T. L. Vincent, Control of a Solid Oxide Fuel Cell System with Sensitivity to Carbon Formation, to appear in: Journal of Power Sources" considers the use of MPC on the SOFC system under load following with constraints. A fourth publication is planned discussing the use of a rate limiter on LPV systems where the system setpoint is one of the measurements included in the scheduling variable.

6.4 Final Remarks

The engineering challenges remaining for SOFC systems currently keep costs very high for what otherwise would be a highly efficient method of energy conversion. Although system control is not a panacea, the ability to operate within temperature and compositional constraints will further decrease the cost of SOFC systems. It is also hoped that this work will provide a useful reference for creation of control driven LPV models for SOFC systems, regardless if the identification is based on a model, or a physical system.

REFERENCES CITED

[1] Thomas A. Adams II and Paul I. Barton. High-efficiency power production from natural gas with carbon capture. *Journal of Power Sources*, 195(7):1971–1983, April 2010. ISSN 03787753. doi: 10.1016/j.jpowsour.2009.10.046. URL http://linkinghub.elsevier.com/retrieve/pii/S0378775309018503.

[2] Ryan O'Hayre, Suk-Won Cha, Whitney Colella, and Fritz B. Prinz. *Fuel Cell Fundamentals*. Wiley, 2005. ISBN 0471741485. URL http://www.amazon.com/Fuel-Cell-Fundamentals-Ryan-OHayre/dp/0471741485.

[3] John Staniforth and R.M. Ormerod. Running solid oxide fuel cells on biogas. *Ionics*, 9(5):336–341, 2003. ISSN 0947-7047. URL http://www.springerlink.com/index/04U1768787221683.pdf.

[4] Matti Noponen, Matias Halinen, Jari Kiviaho, and Jaakko Saarinen. Feasibility of Autothermally Reformed Natural Gas on Anode Supported Solid Oxide Fuel Cells. *Journal of Fuel Cell Science and Technology*, 3(4):438, 2006. ISSN 1550624X. doi: 10.1115/1.2349526. URL http://link.aip.org/link/JFCSAU/v3/i4/p438/s1\&Agg=doi.

[5] E. D. Wachsman and K. T. Lee. Lowering the Temperature of Solid Oxide Fuel Cells. *Science*, 334(6058):935–939, November 2011. ISSN 0036-8075. doi: 10.1126/science.1204090. URL http://www.sciencemag.org/cgi/doi/10.1126/science.1204090.

[6] Benjamin J Spivey, John D Hedengren, and Thomas F Edgar. Constrained Control and Optimization of Tubular Solid Oxide Fuel Cells for Extending Cell Lifetime. In *American Control Conference (ACC), 2012*, pages Page(s): 1356 – 1361, 2012.

[7] R.J. Braun. *Optimal design and operation of solid oxide fuel cell systems for small-scale stationary applications*. PhD thesis, University of Wisconsin, 2002. URL http://minds.wisconsin.edu/handle/1793/7636.

[8] Y.H. Li, S.S. Choi, and S. Rajakaruna. An Analysis of the Control and Operation of a Solid Oxide Fuel-Cell Power Plant in an Isolated System. *IEEE Transactions on Energy Conversion*, 20(2):381–387, June 2005. ISSN 0885-8969. doi: 10.1109/TEC.2005.847998. URL http://ieeexplore.ieee.org/lpdocs/epic03/wrapper.htm?arnumber=1432852.

[9] H Xi, J Sun, and V Tsourapas. A control oriented low order dynamic model for planar SOFC using minimum Gibbs free energy method. *Journal of Power Sources*, 165(1): 253–266, February 2007. ISSN 03787753. doi: 10.1016/j.jpowsour.2006.12.009. URL http://linkinghub.elsevier.com/retrieve/pii/S0378775306025201.

[10] R Kandepu, L Imsland, B Foss, C Stiller, B Thorud, and O Bolland. Modeling and control of a SOFC-GT-based autonomous power system. *Energy*, 32(4):406–417, April 2007. ISSN 03605442. doi: 10.1016/j.energy.2006.07.034. URL http://linkinghub.elsevier.com/retrieve/pii/S036054420600209X.

[11] A. Gebregergis, P. Pillay, D. Bhattacharyya, and R. Rengaswemy. Solid Oxide Fuel Cell Modeling. *IEEE Transactions on Industrial Electronics*, 56(1):139–148, January 2009. ISSN 0278-0046. doi: 10.1109/TIE.2008.2009516. URL http://ieeexplore.ieee.org/lpdocs/epic03/wrapper.htm?arnumber=4682693.

[12] P Aguiar. Anode-supported intermediate temperature direct internal reforming solid oxide fuel cell. I: model-based steady-state performance. *Journal of Power Sources*, 138 (1-2):120–136, November 2004. ISSN 03787753. doi: 10.1016/j.jpowsour.2004.06.040. URL http://linkinghub.elsevier.com/retrieve/pii/S0378775304006950.

[13] Andrew M. Colclasure, Borhan M. Sanandaji, Tyrone L. Vincent, and Robert J. Kee. Modeling and control of tubular solid-oxide fuel cell systems. I: Physical models and linear model reduction. *Journal of Power Sources*, 196(1):196–207, June 2010. ISSN 03787753. doi: 10.1016/j.jpowsour.2010.06.074. URL http://linkinghub.elsevier.com/retrieve/pii/S037877531001061X.

[14] Biao Huang, Yutong Qi, and M. Murshed. Solid Oxide Fuel Cell: Perspective of Dynamic Modeling and Control. In *IFAC International Symposium on Dynamics and Control of Process Systems*, 2010. URL http://www.ualberta.ca/~bhuang/FuelCells/Dycopsl-Huang.pdf.

[15] Fabian Mueller, Jacob Brouwer, Faryar Jabbari, and Scott Samuelsen. Dynamic Simulation of an Integrated Solid Oxide Fuel Cell System Including Current-Based Fuel Flow Control. *Journal of Fuel Cell Science and Technology*, 3(2):144, 2006. ISSN 1550624X. doi: 10.1115/1.2174063. URL http://link.aip.org/link/JFCSAU/v3/i2/p144/s1\&Agg=doi.

[16] A Murshed, B Huang, and K Nandakumar. Control relevant modeling of planer solid oxide fuel cell system. *Journal of Power Sources*, 163(2):830–845, January 2007. ISSN 03787753. doi: 10.1016/j.jpowsour.2006.09.080. URL http://linkinghub.elsevier.com/retrieve/pii/S0378775306020271.

[17] C Stiller, B Thorud, O Bolland, R Kandepu, and L Imsland. Control strategy for a solid oxide fuel cell and gas turbine hybrid system. *Journal of Power Sources*, 158 (1):303–315, July 2006. ISSN 03787753. doi: 10.1016/j.jpowsour.2005.09.010. URL http://linkinghub.elsevier.com/retrieve/pii/S0378775305013248.

[18] F Mueller, F Jabbari, and J Brouwer. On the intrinsic transient capability and limitations of solid oxide fuel cell systems. *Journal of Power Sources*, 187(2):452–460, February 2009. ISSN 03787753. doi: 10.1016/j.jpowsour.2008.11.057. URL http://linkinghub.elsevier.com/retrieve/pii/S0378775308021575.

[19] Jeff S. Shamma and Michael Athens. Gain scheduling: Potential hazards and possible remedies. *Control Systems Magazine, IEEE*, 1992. URL http://ieeexplore.ieee.org/xpls/abs_all.jsp?arnumber=165527.

[20] Matthijs Groot Wassink, Marc van de Wal, Carsten Scherer, and Okko Bosgra. LPV control for a wafer stage: beyond the theoretical solution. *Control Engineering Practice*, 13(2):231–245, February 2005. ISSN 09670661. doi: 10.1016/j.conengprac.2004.03.008. URL http://linkinghub.elsevier.com/retrieve/pii/S0967066104000565.

[21] Yucai Zhu and Zuhua Xu. A method of LPV model identification for control. *Proceedings of the 17th World Congress-IFAC-Seoul, ...*, pages 5018–5023, 2008. URL http://www.nt.ntnu.no/users/skoge/prost/proceedings/ifac2008/data/papers/4064.pdf.

[22] BM Sanandaji, TL Vincent, Andrew Colclasure, and R.J. Kee. Control-Oriented Modeling of a Solid-Oxide Fuel Cell Stack Using an LPV Model Structure. In *Current*. ASME, 2009. URL http://inside.mines.edu/~bmolazem/ASME_final.pdf.

[23] JH Yung. *Gain scheduling for geometrically nonlinear flexible space structures*. PhD thesis, 2001. URL http://18.7.29.232/bitstream/handle/1721.1/16838/51283889.pdf?sequence=1.

[24] Vicenç Puig and Joseba Quevedo. Identification and Control of an Open-flow Canal using LPV Models. *... and Control, 2005 ...*, pages 1893–1898, 2005. URL http://ieeexplore.ieee.org/xpls/abs_all.jsp?arnumber=1582436.

[25] Lennart Ljung. Subspace identification from closed loop data. *Signal Processing*, (1):1–10, 1996. URL http://www.sciencedirect.com/science/article/pii/0165168496000540.

[26] Vincent Verdult. *Nonlinear System Identification : A State-Space Approach*. PhD thesis, University of Twente, 2002.

[27] Michel Verhaegen and Xiaode Yu. A class of subspace model identification algorithms to identify periodically and arbitrarily time-varying systems. *Automatica*, 31(2):201–216, February 1995. ISSN 00051098. doi: 10.1016/0005-1098(94)00091-V. URL http://linkinghub.elsevier.com/retrieve/pii/000510989400091V.

[28] Vincent Verdult and Michel Verhaegen. Kernel methods for subspace identification of multivariable LPV and bilinear systems. *Automatica*, 41(9):1557–1565, September 2005. ISSN 00051098. doi: 10.1016/j.automatica.2005.03.027. URL http://linkinghub.elsevier.com/retrieve/pii/S0005109805001214.

[29] JW Van Wingerden. *Control of wind turbines with'Smart'rotors: proof of concept & LPV subspace identification.* PhD thesis, 2008. URL http://www.narcis.nl/publication/RecordID/oai:tudelft.nl:uuid:21573afa-f9b2-4cb2-96d3-3902328ebe9c.

[30] Marco Sorrentino and Cesare Pianese. Model-based development of low-level control strategies for transient operation of solid oxide fuel cell systems. *Journal of Power Sources*, January 2011. ISSN 03787753. doi: 10.1016/j.jpowsour.2011.01.023. URL http://linkinghub.elsevier.com/retrieve/pii/S0378775311001017.

[31] P. Aguiar, C.S. Adjiman, and N.P. Brandon. Anode-supported intermediate-temperature direct internal reforming solid oxide fuel cellII. Model-based dynamic performance and control. *Journal of Power Sources*, 147(1-2):136–147, September 2005. ISSN 03787753. doi: 10.1016/j.jpowsour.2005.01.017. URL http://linkinghub.elsevier.com/retrieve/pii/S0378775305001473.

[32] Jay T. Pukrushpan, Anna G. Stefanopoulou, and Huei Peng. *Control of fuel cell power systems: principles, modeling, analysis, and ...* Springer, 2004. ISBN 1852338164. URL http://books.google.com/books?hl=en\&lr=\&id=hL5bEVeuhysC\&pgis=1.

[33] Mahshid Fardadi, Fabian Mueller, and Faryar Jabbari. Feedback control of solid oxide fuel cell spatial temperature variation. *Journal of Power Sources*, 195(13):4222–4233, July 2010. ISSN 03787753. doi: 10.1016/j.jpowsour.2009.12.111. URL http://linkinghub.elsevier.com/retrieve/pii/S037877531000039X.

[34] Y. Inui, N. Ito, T. Nakajima, and a. Urata. Analytical investigation on cell temperature control method of planar solid oxide fuel cell. *Energy Conversion and Management*, 47(15-16):2319–2328, September 2006. ISSN 01968904. doi: 10.1016/j.enconman.2005.11.007. URL http://linkinghub.elsevier.com/retrieve/pii/S0196890405003122.

[35] Xiao-Juan Wu, Xin-Jian Zhu, Guang-Yi Cao, and Heng-Yong Tu. Predictive control of SOFC based on a GA-RBF neural network model. *Journal of Power Sources*, 179(1):232–239, April 2008. ISSN 03787753. doi: 10.1016/j.jpowsour.2007.12.036. URL http://linkinghub.elsevier.com/retrieve/pii/S0378775307028005.

[36] Debangsu Bhattacharyya and Raghunathan Rengaswamy. System Identification and Nonlinear Model Predictive Control of a Solid Oxide Fuel Cell. *Industrial & Engineering Chemistry Research*, 49(10):4800–4808, 2010. ISSN 0888-5885. URL http://pubs.acs.org/doi/abs/10.1021/ie9020254.

[37] Borhan M. Sanandaji, Tyrone L. Vincent, Andrew M. Colclasure, and Robert J. Kee. Modeling and control of tubular solid-oxide fuel cell systems: II. Nonlinear model reduction and model predictive control. *Journal of Power Sources*, 196(1): 208–217, July 2010. ISSN 03787753. doi: 10.1016/j.jpowsour.2010.06.075. URL http://linkinghub.elsevier.com/retrieve/pii/S0378775310010621.

[38] Akm M. Murshed, Biao Huang, and K. Nandakumar. Estimation and control of solid oxide fuel cell system. *Computers & Chemical Engineering*, 34(1):96–111, January 2010. ISSN 00981354. doi: 10.1016/j.compchemeng.2009.06.018. URL http://linkinghub.elsevier.com/retrieve/pii/S0098135409001665.

[39] Benjamin J. Spivey and Thomas F. Edgar. Dynamic modeling, simulation, and MIMO predictive control of a tubular solid oxide fuel cell. *Journal of Process Control*, pages 1–19, March 2012. ISSN 09591524. doi: 10.1016/j.jprocont.2012.01.015. URL http://linkinghub.elsevier.com/retrieve/pii/S0959152412000182.

[40] K.J. Kattke, R.J. Braun, a.M. Colclasure, and G. Goldin. High-fidelity stack and system modeling for tubular solid oxide fuel cell system design and thermal management. *Journal of Power Sources*, December 2010. ISSN 03787753. doi: 10.1016/j.jpowsour.2010.12.070. URL http://linkinghub.elsevier.com/retrieve/pii/S0378775310022780.

[41] Olaf Deutschmann, Renate Schwiedernoch, L.I. Maier, and Daniel Chatterjee. Natural gas conversion in monolithic catalysts: interaction of chemical reactions and transport phenomena. *Studies in Surface Science and Catalysis*, 136:251–258, 2001. ISSN 0167-2991. URL http://linkinghub.elsevier.com/retrieve/pii/S0167299101803128.

[42] J Pukrushpan, a Stefanopoulou, S Varigonda, J Eborn, and C Haugstetter. Control-oriented model of fuel processor for hydrogen generation in fuel cell applications. *Control Engineering Practice*, 14(3):277–293, March 2006. ISSN 09670661. doi: 10.1016/j.conengprac.2005.04.014. URL http://linkinghub.elsevier.com/retrieve/pii/S0967066105001371.

[43] Olaf Deutschmann. High temperature catalysis: fundamentals and applications. 2007. URL http://www.itcp.kit.edu/deutschmann/img/content/20070413_Deutschmann_ECM2007_PlenaryLecture_HighTempCatal.pdf.

[44] Alan C Hindmarsh, Peter N Brown, Keith E Grant, Steven L Lee, Radu Serban, Dan E Shumaker, and Carol S Woodward. SUNDIALS: Suite of nonlinear and differential/algebraic equation solvers. *ACM Trans. Math. Softw.*, 31(3):363–396, September 2005. ISSN 0098-3500. doi: 10.1145/1089014.1089020. URL http://doi.acm.org/10.1145/1089014.1089020.

[45] R Schwiedernoch, S Tischer, C Correa, and O Deutschmann. Experimental and numerical study on the transient behavior of partial oxidation of methane in a catalytic monolith. *Chemical Engineering Science*, 58(3-6):633–642, 2003.

[46] DG Goodwin. An open-source, extensible software suite for CVD process simulation. *Chemical Vapor Deposition XVI and EUROCVD*, 14(40):2003–08, 2003. URL http://scholar.google.com/scholar?hl=en\&btnG=Search\&q=intitle:An+Open-Source,+Extensible+Software+Suite+for+CVD+Process+Simulation+D.+G.+Goodwin\#0.

[47] Matthew J. Kupilik and Tyrone L. Vincent. Estimation of biogas composition in a catalytic reactor via an extended Kalman filter. In *Control Applications (CCA), 2011 IEEE International Conference on*, pages 768 – 773, 2011. URL http://ieeexplore.ieee.org/stamp/stamp.jsp?tp=\&arnumber=6044411\&isnumber=6044349.

[48] K.L. Bothi. *Characterization of Biogas from Anaerobically Digested Dairy Waste for Energy Use*. PhD thesis, Cornell University, 2007. URL http://test-dspace.library.cornell.edu/handle/1813/5329.

[49] J Van herle. Biogas as a fuel source for SOFC co-generators. *Journal of Power Sources*, 127(1-2):300–312, March 2004. ISSN 03787753. doi: 10.1016/j.jpowsour.2003.09.027. URL http://linkinghub.elsevier.com/retrieve/pii/S0378775303009649.

[50] R. Kumar Mandela, Raghunathan Rengaswamy, and Shankar Narasimhan. Recursive state estimation techniques for nonlinear differential algebraic systems. *Chemical Engineering Science*, 65(16):4548–4556, 2010. ISSN 0009-2509. doi: 10.1016/j.ces.2010.04.020. URL http://linkinghub.elsevier.com/retrieve/pii/S0009250910002599.

[51] L. Magistri, A. Traverso, A.F. Massardo, and R. K. Shah. Heat Exchangers for Fuel Cell and Hybrid System Applications. *Journal of Fuel Cell Science and Technology*, 3 (2):111, 2006. ISSN 1550624X. doi: 10.1115/1.2173665. URL http://link.aip.org/link/JFCSAU/v3/i2/p111/s1\&Agg=doi.

[52] M Ansari and V Mortazavi. Simulation of dynamical response of a countercurrent heat exchanger to inlet temperature or mass flow rate change. *Applied Thermal Engineering*, 26(17-18):2401–2408, December 2006. ISSN 13594311. doi: 10.1016/j.applthermaleng.2006.02.015. URL http://linkinghub.elsevier.com/retrieve/pii/S1359431106000585.

[53] Wilfried Roetzel and Yimin Xuan. *Dynamic behaviour of heat exchangers*. WIT Press/Computational Mechanics Publications, 1999. ISBN 1853125067. URL http://books.google.com/books?id=vcVvQgAACAAJ\&pgis=1.

[54] S. Gelfi, a.G. Stefanopoulou, and J.T. Pukrushpan. Dynamics of low-pressure and high-pressure fuel cell air supply systems. *Proceedings of the 2003 American Control Conference, 2003.*, pages 2049–2054, 2003. doi: 10.1109/ACC.2003.1243376. URL http://ieeexplore.ieee.org/lpdocs/epic03/wrapper.htm?arnumber=1243376.

[55] A Nakajo, C Stiller, G Harkegard, and O Bolland. Modeling of thermal stresses and probability of survival of tubular SOFC. *Journal of Power Sources*, 158(1):287–294, July 2006. ISSN 03787753. doi: 10.1016/j.jpowsour.2005.09.004. URL http://linkinghub.elsevier.com/retrieve/pii/S0378775305013169.

[56] G.H.J. Broers and B.W. Treijtel. Carbon deposition boundaries and other constant parameter curves, in the triangular representation of CHO equilibria, with applications to fuel cells. *Advanced Energy Conversion*, 5(4):365–382, 1965. ISSN 0365-1789. URL http://linkinghub.elsevier.com/retrieve/pii/036517896590024X.

[57] EJ Cairns and AD Tevebaugh. CHO Gas Phase Compositions in Equilibrium with Carbon, and Carbon Deposition Boundaries at One Atmosphere. *Journal of Chemical & Engineering Data*, 9(3):453–462, 1964. ISSN 0021-9568. URL http://pubs.acs.org/doi/abs/10.1021/je60022a052.

[58] PV Aravind, JP Ouweltjes, E De Heer, and N Woudstra. Impact of Biosyngas and its Components on SOFC Anodes. *Electrochemical Society*, 2005(July), 2005. URL http://www.ecn.nl/docs/library/report/2005/rx05117.pdf.

[59] Siamak Farhad and Feridun Hamdullahpur. Developing fuel map to predict the effect of fuel composition on the maximum efficiency of solid oxide fuel cells. *Journal of Power Sources*, 193(2):632–638, September 2009. ISSN 03787753. doi: 10.1016/j.jpowsour.2009.03.054. URL http://linkinghub.elsevier.com/retrieve/pii/S0378775309005552.

[60] Siamak Farhad and Feridun Hamdullahpur. Developing fuel map to predict the effect of fuel composition on the maximum voltage of solid oxide fuel cells. *Journal of Power Sources*, 191(2):407–416, June 2009. ISSN 03787753. doi: 10.1016/j.jpowsour.2009.02.073. URL http://linkinghub.elsevier.com/retrieve/pii/S0378775309003711.

[61] Jan-Willem van Wingerden and Michel Verhaegen. Subspace identification of Bilinear and LPV systems for open- and closed-loop data. *Automatica*, 45(2):372–381, February 2009. ISSN 00051098. doi: 10.1016/j.automatica.2008.08.015. URL http://linkinghub.elsevier.com/retrieve/pii/S0005109808004743.

[62] I. Houtzager, P.M.O. Gebraad, J. Van Wingerden, and M. Verhaegen. Predictor-based Subspace Identification Toolbox Version 0.5, 2012. URL http://www.dcsc.tudelft.nl/~datadriven/pbsid/.

[63] H.B. Huo, X.J. Zhu, W.Q. Hu, H.Y. Tu, Jian Li, and Jie Yang. Nonlinear model predictive control of SOFC based on a Hammerstein model. *Journal of Power Sources*, 185(1):338–344, October 2008. ISSN 03787753. doi: 10.1016/j.jpowsour.2008.06.064. URL http://linkinghub.elsevier.com/retrieve/pii/S0378775308012706.

[64] Alberto Bemporad. Robust model predictive control: A survey. *Robustness in identification and control*, 1999. URL http://www.springerlink.com/index/n8734746605j8447.pdf.

[65] Thomas Besselmann and J Lofberg. Explicit model predictive control for linear parameter-varying systems. *Control, 2008. CDC 2008.*, (1):3848–3853, 2008. URL http://ieeexplore.ieee.org/xpls/abs_all.jsp?arnumber=4738798.

[66] Thomas Besselmann. Explicit MPC for LPV Systems: Stability and Optimality. *Automatic Control, IEEE ...*, 57(9):2322–2332, 2012. URL http://ieeexplore.ieee.org/xpls/abs_all.jsp?arnumber=6151042.

[67] M Kvasnica, P Grieder, M Baoti, and M Morari. Multi-parametric toolbox (MPT), 2004. URL http://control.ee.ethz.ch/~mpt/.

[68] John Doyle, Bruce Francis, and Allen Tennenbaum. *Feedback Control Theory*. 1992. ISBN 0-02-330011-6.